6469-EE-01

LIGHT SCATTERING FROM ROUGH SURFACES

Principal Investigator: J C Dainty
Contractor: Imperial College
Contract Number: DAJA45-90-C-0026

Final Report

(Report Date: 17th August 1994)

"The research reported in this document has been made possible through the support and sponsorship of the US Government through its European Research Office of the US Army. The report is intended only for the internal management use of the Contractor and the US Government."

LIGHT SCATTERING FROM ROUGH SURFACES

FINAL REPORT

EXECUTIVE SUMMARY

The particular aspect of light scattering investigated in this project was the angular correlation of speckle patterns produced by scattering from rough surfaces. The Report consists primarily of a draft copy of the Thesis of R J Syratt, the student employed on the Contract.

A randomly rough surface illuminated by a parallel laser beam at some angle θ produces a speckle pattern in space. If the angle of illumination is changed to $\theta + \delta\theta$ then the speckle pattern changes in two ways: (i) it translates in angle and (ii) it changes its pattern in a manner that depends on the detailed surface characteristics and the angles involved. We have made experimental measurements of the angular correlation of speckle for two-dimensional Gaussian surfaces of low and high root-mean-square slope. In comparing with theory we have distinguished between surfaces for which single scattering is valid (very low slope) and those for which Kirchhoff theory is valid (larger rms slopes). A numerical ray-tracing approach has been implemented for two-dimensional surfaces that includes shadowing and polarisation in a limited way. A conceptual, heuristic model is developed that explains the essential physical features.

In addition to the main subject of this study, we also investigated a number of subsidiary topics as detailed in the attached publications.

PUBLICATIONS

1 N C Bruce and J C Dainty, "Multiple scattering from rough dielectric and metal surfaces using the Kirchoff approximation", J Mod Optics, **38**, 1471 - 1481 (1991)

2 R W Syratt and J C Dainty, "Angular correlation of speckle patterns", Poster Paper, ICO Topical Meeting on Atmospheric, Volume and Surface Scattering and Propagation, Florence, August 27-30, 1991

3 J C Dainty, N C Bruce and A J Sant, "Measurements of light scattering by a characterised random rough surface", Waves in Random Media, **3**, S29 - S39 (1991)

4 N C Bruce, A J Sant and J C Dainty, "The Mueller matrix for rough surface scattering using the Kirchhoff approximation", Opt Commun, **88**, 471 - 484 (1992)

5 R W Syratt and J C Dainty, "Theory and measurements of the angular correlation of speckle patterns", Paper OP5.3, Applied Optics and Opto-Electronics, Leeds, 14 - 17 September 1992

6 N C Bruce, "Scattering from dense volumes", Paper OP1.5, Applied Optics and Opto-Electronics, Leeds, 14 - 17 September 1992

7 V Ruiz-Cortés and J C Dainty, "Measurements of angular scattering by rough surfaces at grazing incidence", presented at ICO-16, Budapest, 9 - 13 August 1993

8 N C Bruce, V Ruiz-Cortés and J C Dainty, "Calculations of grazing incidence scattering from random rough surfaces using the Kirchhoff approximation", Opt Commun, **106**, 123 - 126 (1994)

JOURNAL OF MODERN OPTICS, 1991, VOL. 38, NO. 8, 1471–1481

Multiple scattering from rough dielectric and metal surfaces using the Kirchhoff approximation

N. C. BRUCE and J. C. DAINTY
The Blackett Laboratory, Imperial College,
London SW7 2BZ, England

(*Received 11 January 1991*)

Abstract. The Kirchhoff double-scatter method for calculating the intensity distribution scattered from a rough surface is extended to dielectric and metal surface materials. The material properties are contained in the Fresnel reflection coefficients only. It is shown that the results agree well with calculations using the exact method for a surface of Gaussian statistics with standard deviation of height $\sigma = 1{\cdot}93\lambda$ and $1/e$ correlation length $\tau = 5{\cdot}02\lambda$.

1. Introduction

In a previous paper [1] it was shown that using the Kirchhoff approximation (KA) and including shadowing, it was possible to derive equations for the single- and double-scatter contributions to the intensity distribution scattered from a randomly rough surface. In [1], the simplest situation was considered—that of a perfectly conducting surface. As expected, the double-scatter term showed the enhanced backscatter effect [2–4], with a peak approximately equal to twice the background in the backscatter direction. This agrees with the simple ray picture of the scattering process for which rays and their time-reversed partners add coherently in the backscatter direction and incoherently in other directions.

A comparison of the perfect conductor calculations with experimental distributions of the scattered light from a gold-coated surface with Gaussian statistics showed good agreement at low angles of incidence (up to about 20° from normal) but poor agreement at higher angles [1]. The same trend is seen in comparisons of exact calculations using the extinction theorem with experimental values [4], although for perfectly conducting surfaces the calculated intensities for the extinction and Kirchhoff double-scatter methods agree very well [5]. This suggests that the Kirchhoff method has included the main physical processes that produce enhanced backscatter.

In this paper the results of the method for the more general cases of scattering from a dielectric and a general conductor (metal) are reported. In section 2 the theory is briefly outlined and in section 3 the results are shown and compared with exact calculations and experimental results.

2. Theory

The starting point is the two-dimensional Helmholtz integral equation for a scattered field (the surface profile is constant along the y-direction):

$$E_s(x,z) = \frac{1}{4\mathrm{i}} \int_\Gamma \left(E_t(x',z') \frac{\partial H_0^{(1)}(kr)}{\partial n} - H_0^{(1)}(kr) \frac{\partial E_t(x',z')}{\partial n} \right) \mathrm{d}s', \qquad (1)$$

0950-0340/91 $3·00

where $E_t(x', z')$ is the total field at the point (x', z'), $r=[(x-x')^2+(z-z')^2]^{1/2}$, $H_0^{(1)}(kr)$ is the zeroth order Hankel function of the first kind and ds' is an element of the surface.

The KA approximates the total field on the surface as the sum of the incident field plus the reflected field at that point:

$$E_t(x, z)=(1+R)E_i(x, z), \tag{2}$$

$$\frac{\partial E_t(x, z)}{\partial n}=i(1-R)\mathbf{k}_i\cdot\mathbf{n}E_i(x, z), \tag{3}$$

where R is the planar reflection coefficient at that point, depending on the local incidence angle; $E_i(x, z)$ is the field incident at that point; $\mathbf{k}_i$ is the incident wavevector; and $\mathbf{n}$ is the outward normal to the surface at the point (x, z). Since R is the planar reflection coefficient, we immediately have a condition for the validity of the approximation—the surface must be locally flat or, as is usually written, the radius of curvature of the surface must be large compared with the wavelength.

Substituting (2) and (3) into (1) and performing a small amount of mathematics, following Beckmann and Spizzichino [6], the standard single-scatter solution is obtained:

$$E_s(\theta)=-\left(\frac{2}{\pi kr}\right)^{1/2}\frac{\exp i\varphi}{2}\frac{1+\cos(\theta+\theta_i)}{\cos\theta+\cos\theta_i}\int_\Gamma R(x', z')\exp i(\mathbf{k}_i-\mathbf{k})\cdot\mathbf{R}\,dx', \tag{4}$$

where the reflectivity is a function of x, since the local angle of incidence varies along the surface. In equation (4), θ_i is the incidence angle, θ is the angle of scatter (measured positive in the opposite direction to the incident angle) and φ is a phase factor depending only on (x, z) and not on (x', z'). To obtain this expression we have assumed an incident plane wave of unit amplitude. Shadowing effects must somehow be included in this method to have a physically realistic result. This is done by multiplying the integrand in (4) by incidence and scatter shadow functions

$$S(x', z')=\begin{cases}1 & \text{if } (x', z') \text{ is illuminated,}\\ 0 & \text{if } (x', z') \text{ is not illuminated,}\end{cases}$$

$$S'(x', z')=\begin{cases}1 & \text{if } (x', z') \text{ is visible,}\\ 0 & \text{if } (x', z') \text{ is not visible.}\end{cases}$$

These represent geometrical or straight line shadow functions and so are an approximation to the true effect of shadowing.

The derivation of the double-scatter contribution involves two terms. The first is the field scattered from one point on the surface to another point, also on the surface,

$$E_s(x_2, z_2)=\frac{1}{4i}\left((1+R_1)\left(m_1\frac{k(x_2-x_1)}{r_{12}}-\frac{k(z_2-z_1)}{r_{12}}\right)H_1^{(1)}(kr_{12})\right.$$

$$\left.-(1-R_1)ik(m_1\sin\theta_i+\cos\theta_i)H_0^{(1)}(kr_{12})\right)E_i(x_1, z_1), \tag{5}$$

where subscript 1 represents the first point and subscript 2 the second. The normal derivative of the Hankel function is given by

$$\frac{\partial H_0^{(1)}(kr_{12})}{\partial n}=\left[n_x\frac{k(x_2-x_1)}{r_{12}}+n_z\frac{k(z_2-z_1)}{r_{12}}\right]H_1^{(1)}(kr_{12}). \tag{6}$$

The second term is the field scattered into the space above the surface from every combination of first and second points:

$$E_s^2(\theta)=-\left(\frac{2}{\pi kr}\right)^{1/2}\frac{\exp i\varphi}{4}\int_{\Gamma_1}\int_{\Gamma_2}S_{12}''\Big((1+R_2)k(m_2\sin\theta-\cos\theta)E_s(x_2,z_2)$$
$$+i(1-R_2)\frac{\partial E_s(x_2,z_2)}{\partial n_2}\Big)\exp i\mathbf{k}\cdot\mathbf{R}_2\,dx_1\,dx_2, \tag{7}$$

where we have included another shadowing function to describe shadowing between points on the surface:

$$S_{12}=\begin{cases}1 & \text{if } (x_2,z_2) \text{ is visible from } (x_1,z_1),\\ 0 & \text{if } (x_2,z_2) \text{ is not visible from } (x_1,z_1),\end{cases}$$

and substituted

$$S_{12}''=S(x_1,z_1)S_{12}S'(x_2,z_2).$$

In equation (7) we have used equation (2) a second time to write that the total field at the second point is the field from the first point plus its reflection (R_2). This can be seen to be reasonable if it is noted that the condition on the radius of curvature depends only on the surface profile and so will be true for all subsequent interactions if it is true for the first. The validity of the parameters used here was discussed in the previous paper. This method is the same as the iterative Kirchhoff solution [7, 8] but with the inclusion of the shadow functions giving the effect of shadowing explicitly rather than implicitly as in the iterative method [8].

Equations (5) and (7) together form the double-scatter contribution. The simplest case to consider is when the material is perfectly conducting. Then the reflection coefficients R are either 1 or -1 for p (TM) and s (TE) polarizations, respectively, and we are left with only one term as already discussed. For the more general case we end up with the sum of four terms. In all the cases considered, the normal derivative $\partial E_s(x_2,z_2)/\partial n_2$ is approximated in the following way:

$$\frac{\partial E_s(x_2,z_2)}{\partial n_2}=-\frac{1}{4i}\Big((1+R_1)\Big(m_1\frac{k(x_2-x_1)}{r_{12}}-\frac{k(z_2-z_1)}{r_{12}}\Big)\frac{\partial H_1^{(1)}(kr_{12})}{\partial n_2}$$
$$-(1-R_1)ik(m_1\sin\theta_i+\cos\theta_i)\frac{\partial H_0^{(1)}(kr_{12})}{\partial n_2}\Big)E_i(x_1,z_1). \tag{8}$$

In (8) we need to use

$$\frac{\partial H_1^{(1)}(kr_{12})}{\partial n_2}=\Big[n_{2x}\frac{k(x_2-x_1)}{r_{12}}+n_{2z}\frac{k(z_2-z_1)}{r_{12}}\Big]\frac{1}{2}[H_0^{(1)}(kr_{12})-H_2^{(1)}(kr_{12})].$$

The material dependence of these equations is contained solely in the Fresnel reflection coefficients R. For scattering from a dielectric surface of refractive index n in air ($n=1$), the reflection coefficients for p and s polarizations are [9]

$$R_p=\frac{n\cos\theta_i-\sqrt{\left(1-\dfrac{\sin^2\theta_i}{n^2}\right)}}{n\cos\theta_i+\sqrt{\left(1-\dfrac{\sin^2\theta_i}{n^2}\right)}}, \tag{9}$$

$$R_s=\frac{\cos\theta_i-n\sqrt{\left(1-\frac{\sin^2\theta_i}{n^2}\right)}}{\cos\theta_i+n\sqrt{\left(1-\frac{\sin^2\theta_i}{n^2}\right)}}. \tag{10}$$

To find the scattered field we substitute either (9) or (10), depending on the polarization, into (5) and (7). This case of the perfect dielectric is reasonably straightforward. A more complicated situation occurs when the case of light scattered from an interface between a dielectric and air is considered when the light is incident from the dielectric side of the boundary. In this case the Fresnel coefficients are [9]

$$R_p=\frac{\cos\theta_i-n\sqrt{1-n^2\sin^2\theta_i}}{\cos\theta_i+n\sqrt{1-n^2\sin^2\theta_i}}, \tag{11}$$

$$R_s=\frac{n\cos\theta_i-\sqrt{1-n^2\sin^2\theta_i}}{n\cos\theta_i+\sqrt{1-n^2\sin^2\theta_i}}. \tag{12}$$

Then, when

$$n^2\sin^2\theta_i>1,$$

the reflectivities are complex. This occurs when the critical incidence angle θ_c is reached and we have total internal reflection

$$\theta_c=\sin^{-1}\left(\frac{1}{n}\right).$$

The final case considered is that of the general conductor or metal which involves a complex refractive index $n\rightarrow n+i\kappa$. In this case the reflectivities are [9]

$$R_p=\frac{(n^2\cos^2\theta_i-q^2\cos^2\gamma)+(\kappa^2\cos^2\theta_i-q^2\sin^2\gamma)}{(n\cos\theta_i+q\cos\gamma)^2+(\kappa\cos\theta_i+q\sin\gamma)^2}$$
$$+2i\frac{(\kappa q\cos\theta_i\cos\gamma-nq\sin\gamma\cos\theta_i)}{(n\cos\theta_i+q\cos\gamma)^2+(\kappa\cos\theta_i+q\sin\gamma)^2}, \tag{13}$$

$$R_s=\frac{\cos^2\theta_i-(nq\cos\gamma-\kappa q\sin\gamma)^2-(\kappa q\cos\gamma+nq\sin\gamma)^2}{(\cos\theta_i+(nq\cos\gamma-\kappa q\sin\gamma))^2+(\kappa q\cos\gamma+nq\sin\gamma)^2}$$
$$-2i\frac{\cos\theta_i(\kappa q\cos\gamma+nq\sin\gamma)}{(\cos\theta_i+(nq\cos\gamma-\kappa q\sin\gamma))^2+(\kappa q\cos\gamma+nq\sin\gamma)^2}, \tag{14}$$

where

$$q^4=\left(1-\frac{(n^2-\kappa^2)}{(n^2+\kappa^2)}\sin^2\theta_i\right)^2+\left(\frac{2n\kappa}{(n^2+\kappa^2)^2}\sin^2\theta_i\right)^2, \tag{15}$$

$$\tan 2\gamma=\frac{\left(1-\frac{(n^2-\kappa^2)}{(n^2+\kappa^2)}\sin^2\theta_i\right)}{\frac{2n\kappa}{(n^2+\kappa^2)^2}\sin^2\theta_i}. \tag{16}$$

It should be noted that the contribution from light paths that traverse inside parts of the surface are not taken into account. It is believed that such terms are small due to the requirement for large angles of deviation of refraction to direct light back into the space above the surface.

3. Results

The Kirchhoff method equations have been discretised in the usual way (assuming that values of parameters remain constant over a suitably small range of variables) and programmed into a Sun 4 computer. A surface of length 30λ was discretized into 200 segments giving a segment length of $0{\cdot}15\lambda$. Computation times were 7 minutes per frame for the dielectric cases and 10 minutes per frame for the metal with approximately 600 frames averaged for each graph. Computational results are shown in figure 1 with experimental results [10] shown in figure 2 for comparison. The surface parameters are: standard deviation of height $\sigma = 1{\cdot}18\,\mu m$, correlation length $\tau = 2{\cdot}97\,\mu m$, with a wavelength of $0{\cdot}633\,\mu m$ (He–Ne red) and a refractive index of $n = 1{\cdot}41$. The scattered energy as a function of incidence angle for both methods is given in table 1.

The Kirchhoff and exact methods agree quite well both for scattered energy and the intensity distribution up to $-30°$ incidence. In both the s and p cases the Kirchhoff scattered intensity distribution is rising at scatter angles near $+90°$ and for p-polarization the energy scattered is twice its value for the extinction case. The cause of this may be that the effect of light paths that pass through the material are becoming important, or the approximation used for the shadow functions, i.e. straight line or geometric shadow functions, is less valid when incidence shadowing starts to have an effect. The second reason is supported by the fact that for the perfectly conducting case the unitarity was from 6 to 9% greater than unity. There is reasonable agreement with the shape of the experimental curves, although note that the experimental values have not been normalized. However, from the Kirchhoff results it can be seen that the double-scattered energy is an order of magnitude down on the single scatter for s-polarization (TE) and several orders of magnitude down for p-polarization (TM). This means that scattering from this dielectric surface is mainly a single-scatter effect, so that even though enhanced backscatter can be seen in the double-scatter curves, the effect on the total scatter curve is very small. This is probably because only a small part of the energy is reflected at each interaction point on the surface.

Assuming that in this single-scatter regime the dominant term from each part of the surface is the specular term it can be shown that the minimum in the p-polarization case is directly related to the Brewster angle. Figure 3 shows the situation where one of the discretized surface facets is illuminated at the Brewster angle and so will not scatter p-polarized light. Then θ_s, the scatter angle, is given by

$$-\theta_s = \theta_i + 2\theta_B,$$

since θ_i is negative. For $n = 1{\cdot}41$, the Brewster angle is

$$\theta_B = \tan^{-1}(1{\cdot}41) \approx 55°.$$

Thus at $\theta_i = -30°$, $\theta_s = -80°$ and at $\theta_i = -60°$, $\theta_s = -50°$, which agrees reasonably well with the observed angle at which the minimum occurs. Another feature of the curves which can be explained using the single-scatter model is that the s and p curves have the same value at backscatter for all incidence angles. If the specular term is dominant then the backscatter results from parts of the surface which are normal to the incident direction. The Fresnel coefficients for normal reflections have the same modulus but different sign for s and p, so the scattered intensities are the same in the backscatter direction.

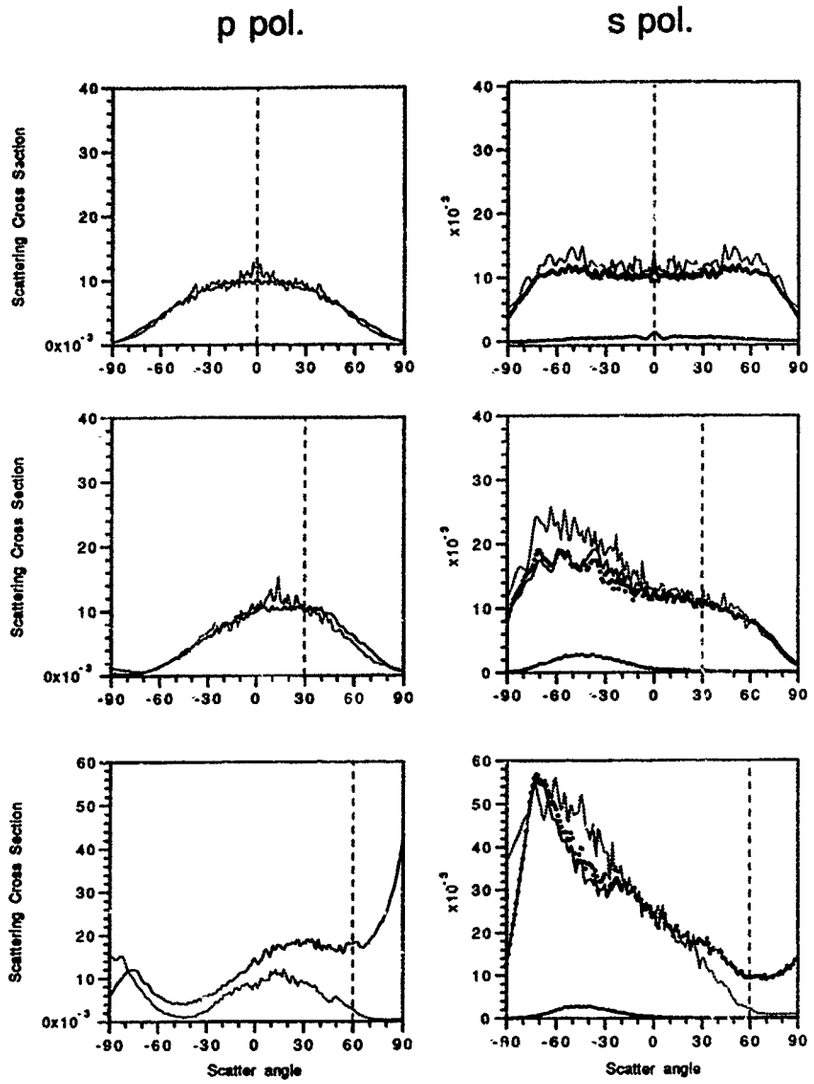

Figure 1. Scattering cross-section as a function of angle for p (right) and s polarization, 0° (top), −30° (middle) and −60° incidence from a dielectric surface $n=1{\cdot}41$ with $\sigma=1{\cdot}18\,\mu m$ and $\tau=2{\cdot}97\,\mu m$. Kirchhoff total (solid line), single (oooo), double (++++) and extinction calculation (dotted line). Backscatter is marked by the vertical dashed line.

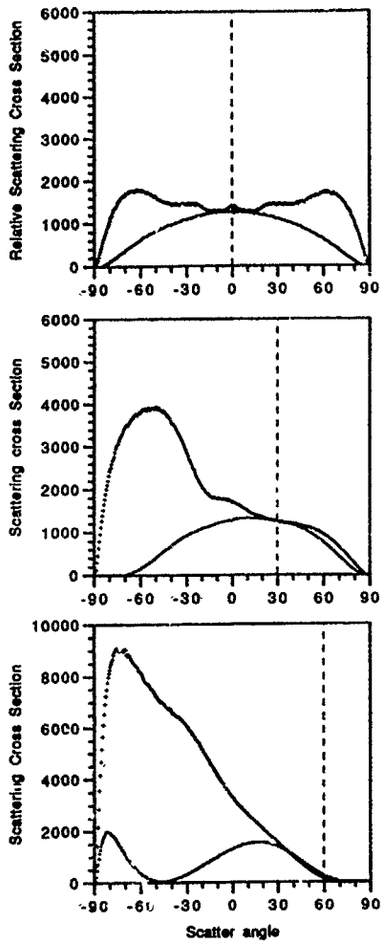

Figure 2. Experimental curves for scattering from a dielectric as in figure 1: s (upper curve) and p (lower curve) polarizations.

Table 1. Scattered energy as a function of incidence angle (dielectric).

Incidence angle	Kirchhoff single	Kirchhoff double	Kirchhoff total	Exact
s-polarization (TE)				
0°	0·031	0·0012	0·031	0·035
−30°	0·037	0·0028	0·038	0·043
−60°	0·081	0·0022	0·079	0·080
p-polarization (TM)				
0°	0·018	0·0001	0·0180	0·020
−30°	0·018	0·0001	0·0181	0·018
−60°	0·043	0·0002	0·043	0·018

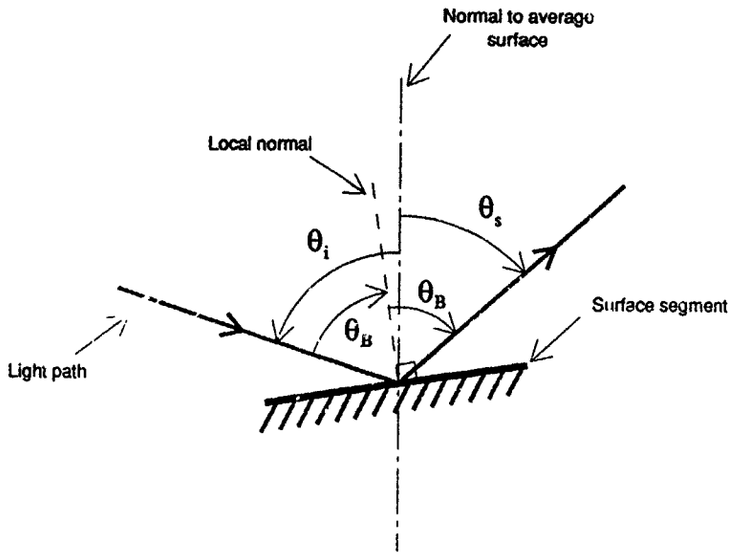

Figure 3. Geometry for scattering at Brewster angle.

The results for the inverse dielectric case for the Kirchhoff method with s-polarization and the same material as above ($n=1{\cdot}41$) are shown in figure 4. The scattered energy is shown in table 2.

In this case, the double scatter forms a much larger part of the total scattered energy so that a strong enhanced backscatter peak is expected. Indeed, this is seen at low angles of incidence but the peak dies away quickly so that by $-20°$ it has almost disappeared completely. The steep slope of the double-scatter curve between 0° and 20° gives this effect.

The peak in the single-scatter curves at large negative angles can be explained in the same way as the Brewster angle effect above. The scatter angle corresponding to a local angle of incidence equal to the critical angle is given by

$$-\theta_s=\theta_i+2\theta_c,$$

where the critical angle θ_c is given by

$$\theta_c=\sin^{-1}\left(\frac{1}{n}\right)\approx 45°,$$

giving $\theta_s=-70°$ for $\theta_i=-20°$. This angle should give the start of the region of total internal reflection. Shadowing counteracts this effect by blocking light scattered at high angles, causing the reflectivities to come down again toward $-90°$.

The final case considered is that of scattering from a metal, in particular gold, at $\lambda=0{\cdot}633\,\mu m$, with the refractive index $n=0{\cdot}167+i3{\cdot}149$ [11]. Previous comparisons of experiment and theory have used calculations from perfect conductors, so it would be useful to find the effect of finite conductivity on the scattered intensity. The scattered energy for two angles of incidence is given in table 3.

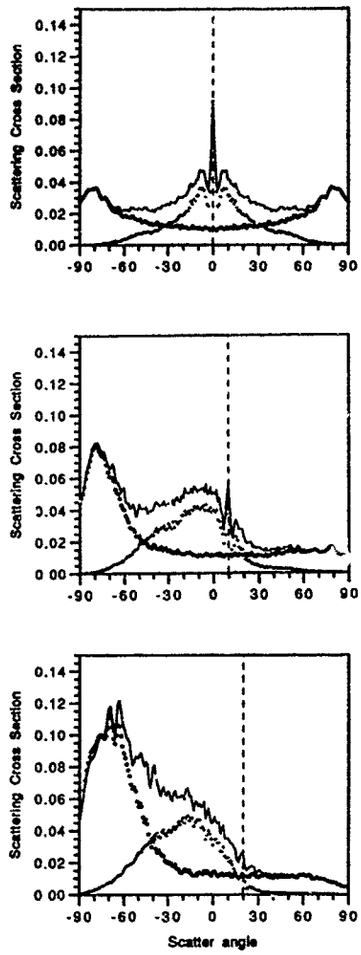

Figure 4. As figure 1, for scattering from a dielectric–air interface from the dielectric side: 0° (top), −10° (middle) and −20° incidence angles.

Table 2. Scattered energy (inverse dielectric).

Incidence angle	Kirchhoff single	Kirchhoff double	Kirchhoff total
0°	0·058	0·037	0·095
−10°	0·070	0·043	0·114
−20°	0·097	0·050	0·148

Table 3. Scattered energy for two different angles of incidence (gold).

Incidence angle	Kirchhoff single	Kirchhoff double	Kirchhoff total
s-polarization (*TE*)			
0°	0·811	0·105	0·902
−40°	0·847	0·075	0·872
p-polarization (*TM*)			
0°	0·783	0·112	0·882
−40°	0·829	0·069	0·849

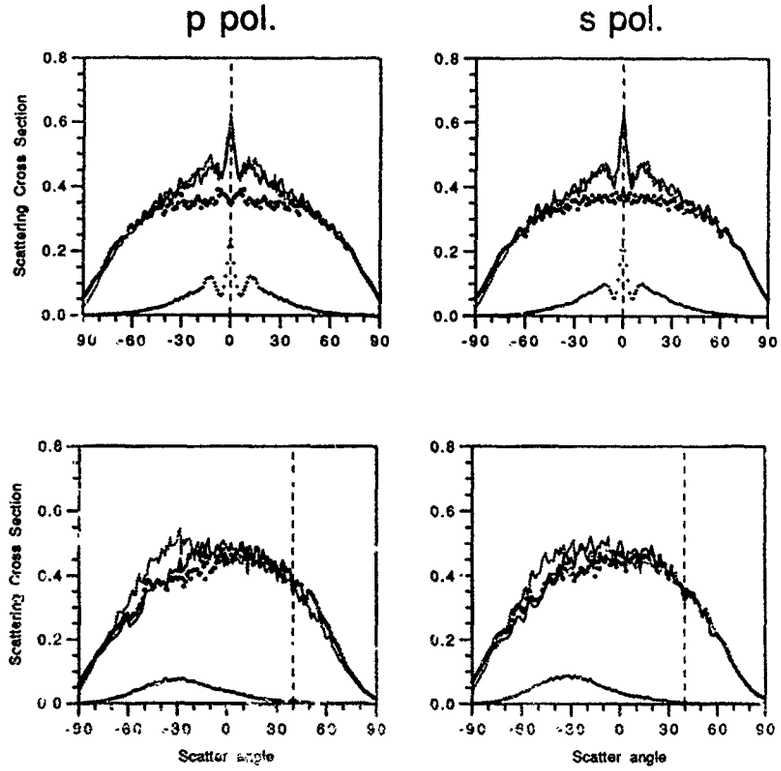

Figure 5. As figure 1, for a metal surface at 0° (top) and −40° incidence. Kirchhoff total (solid line), single (oooo) and double (++++) renormalized to have unit area under the total curve. The dotted line is the Kirchhoff total for the same surface as a perfect conductor.

These values of scattered energy could be used as a check on the parameters of the surface material, allowing a check on whether there is an unexpected effect present in the scattering process, for example, if the metal coating is too thin or if there is some granulation of the surface material. Here, to compare the perfect conductor and metal results, the two cases are normalized to the same area under the graph (as has been done on previous experimental results) and compared directly. Figure 5 shows the results. There is very little difference in the metal and perfectly conducting curves, showing that finite conductivity has very little effect on the scattered intensity distribution.

4. Conclusions

Using the Kirchhoff double-scatter contribution it has been shown that scattering from a particular dielectic surface is mainly a single-scatter effect when the light is incident from the air side, but when the incidence is from the dielectric side much more light is double scattered. We believe that the reflectivities at each interaction are very low in the first case and total internal reflection gives relatively more double scattering in the second. The results agree well with exact calculations using the extinction theorem, except at higher angles of incidence where it is thought that the approximation used for shadowing becomes less valid. Scattering from a metal surface was compared with scattering from a perfect conductor and found to agree well. This shows that the effect of finite conductivity, at least for very good conductors, is purely to reduce the scattered energy and not to alter the scattered intensity distribution.

Acknowledgments

This work was supported by the Royal Signals and Radar Establishment (Malvern), the U.K. Science and Engineering Research Council (GR/F 81651) and the U.S. Army (DAJA45-90-0026).

References

[1] Bruce, N. C., and Dainty, J. C., 1991, *J. mod. Optics*, **38**, 579.
[2] Mendez, E. R., and O'Donnell, K. A., 1987, *Optics Commun.*, **61**, 91.
[3] O'Donnell, K. A., and Mendez, E. R., 1987, *J. opt. Soc. Am. A*, **4**, 1194.
[4] Kim, M.-J., Dainty, J. C., Friberg, A. T., and Sant, A. J., 1990, *J. opt. Soc. Am.* A, **7**, 569.
[5] Dainty, J. C., Bruce, N. C., and Sant, A. J., 1991, *Waves in Random Media* (submitted for publication).
[6] Beckmann, P., and Spizzichino, A., 1963, *The Scattering of Electro-magnetic Waves from Rough Surfaces* (New York: Pergamon).
[7] Brown, G. S., 1984, *Radio Science*, **19**, 1461.
[8] Liszka, E. G., and McCoy, J. J., 1982, *J. Acoust. Soc. Am.*, **71**, 1093.
[9] Born, M., and Wolf, E., 1987, *Principles of Optics* (Oxford: Pergamon).
[10] Sant, A. J., Dainty, J. C., and Kim, M.-J., 1989, *Optics Lett.*, **14**, 1183.
[11] Palik, E. D. (ed.), 1985, *Handbook of Optical Constants of Solids* (London: Academic).

Angular Correlation of Speckle Patterns

R W Syratt and J C Dainty
(Imperial College)

Presented at the ICO Topical Meeting on
Atmospheric, Volume and Surface Scattering and Propagation
Florence, August 27-30, 1991

Geometry

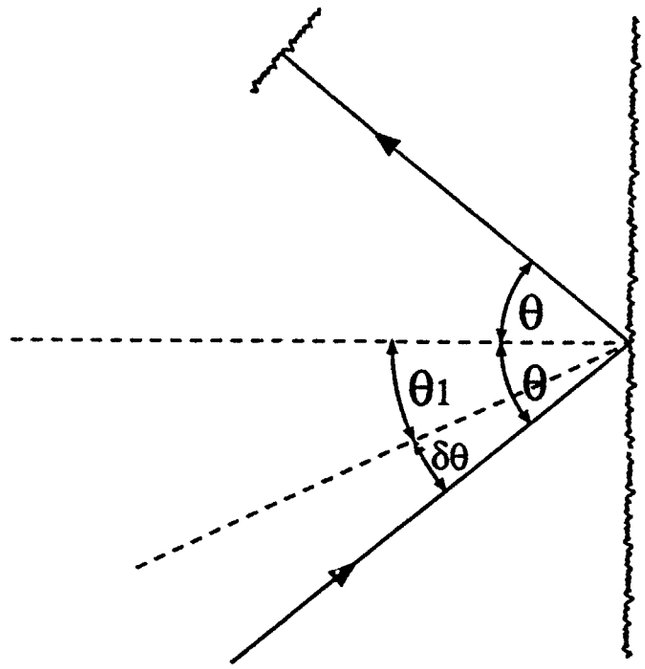

$$\theta = \theta_1 + \delta\theta$$

Kirchhoff Prediction

Correlation:

$$\langle E(\delta\theta)\rangle = \exp\left[-(2k\sigma)^2(\cos\theta_1-\cos(\theta_1+\delta\theta))^2\right]$$

Where σ is the RMS surface height.

k is $(2\pi/\lambda)$

λ is 633 nm for all graphs

See also "Real-time measurement of surface roughness by correlation of speckle patterns"
D. Léger and J.C. Perrin.
J. Opt. Soc. Am., Vol. 66, No. 11, November 1976

Experimental Setup

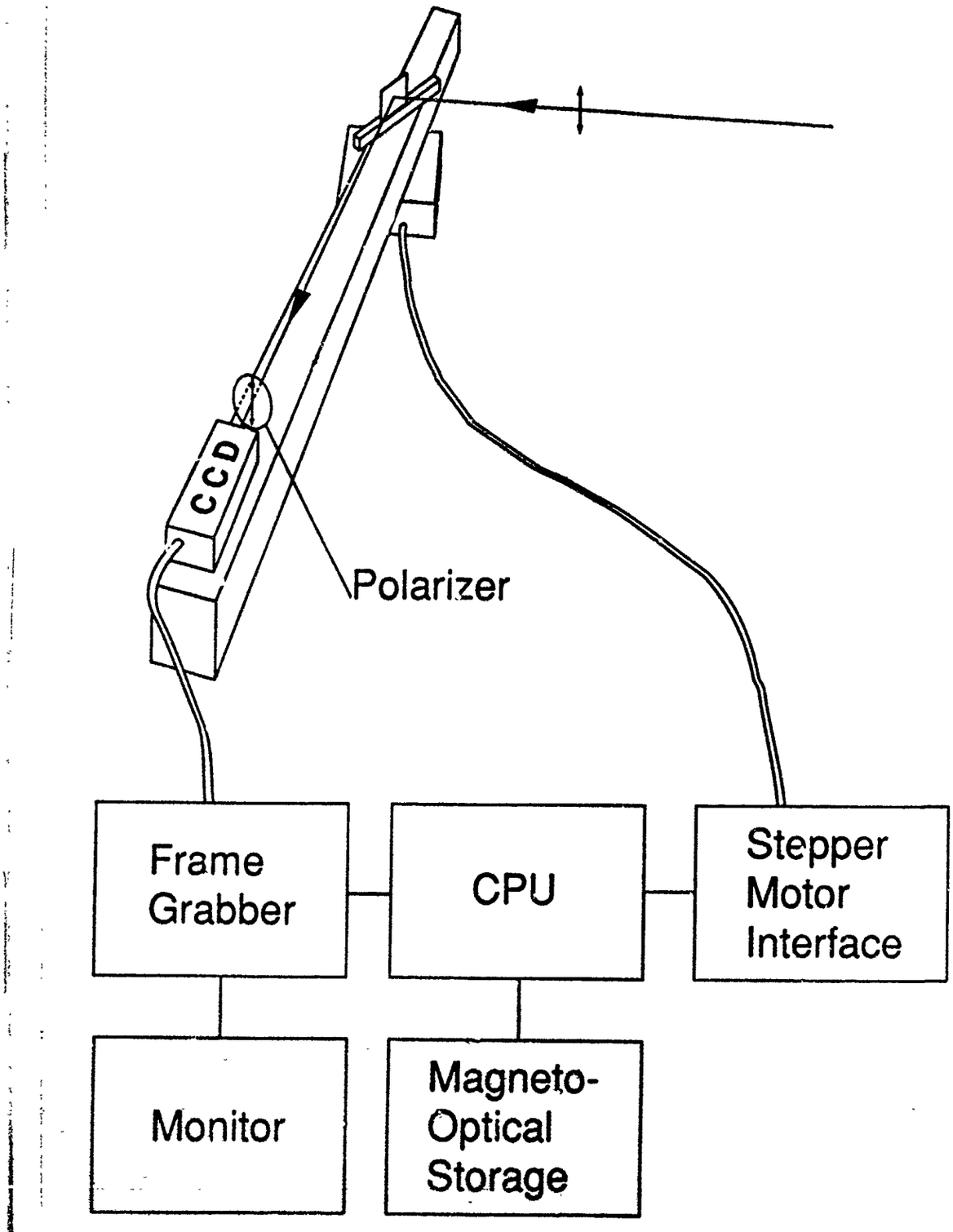

Angular Correlation for surface A
Experimental (markers)and Theory (lines).
RMS Hieght 2.3 μm, (Correlation Length 20.9 μm).

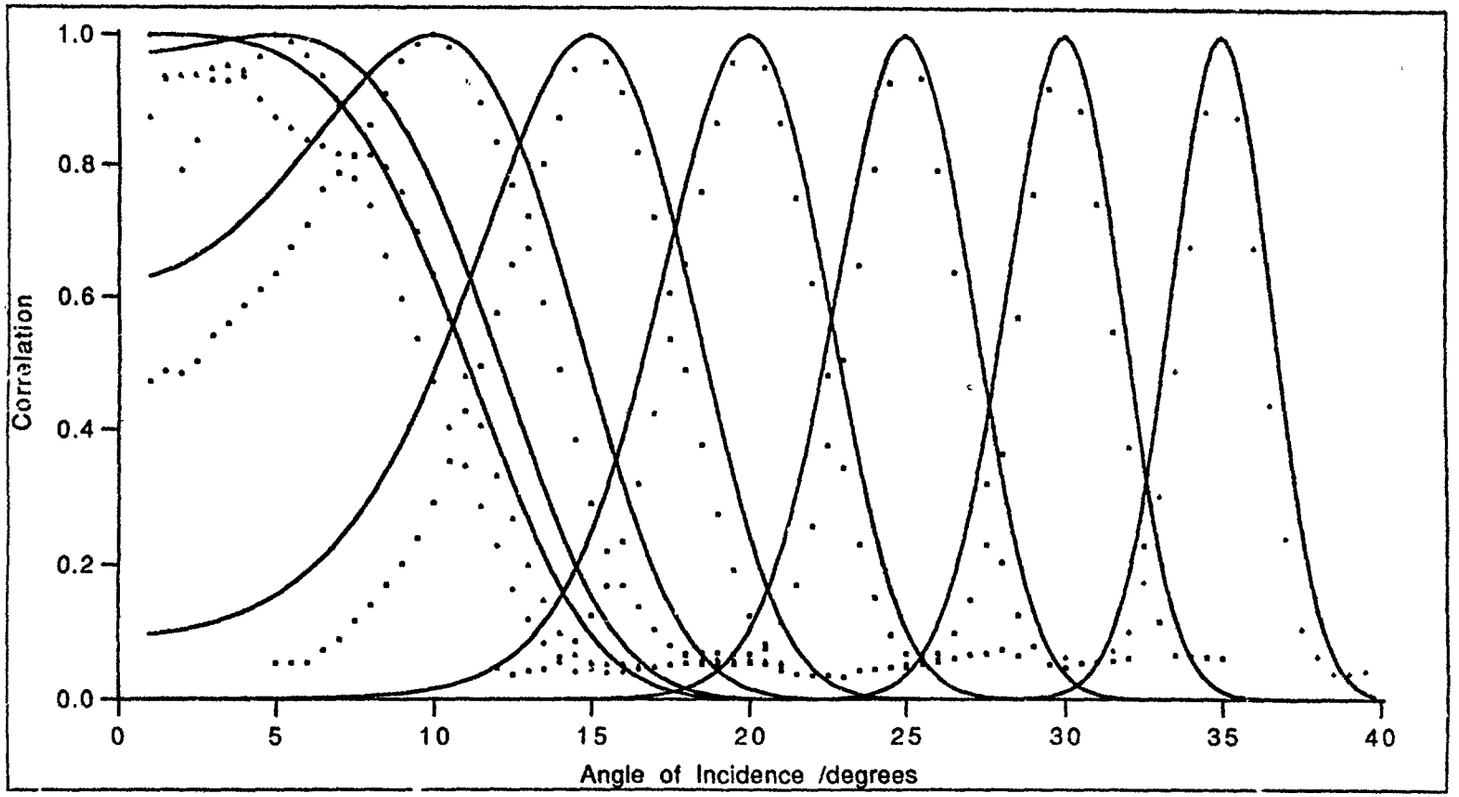

Angular Correlations for Surfaces of Differing Statistics

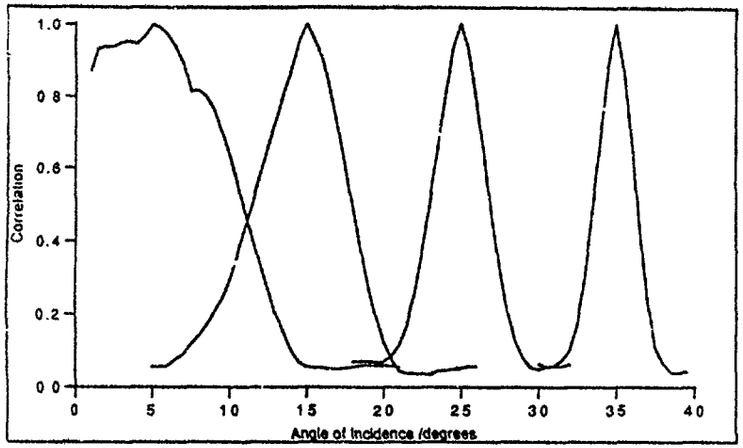

Surface A, RMS Height 2.3 μm, Correlation Length 20.9 μm

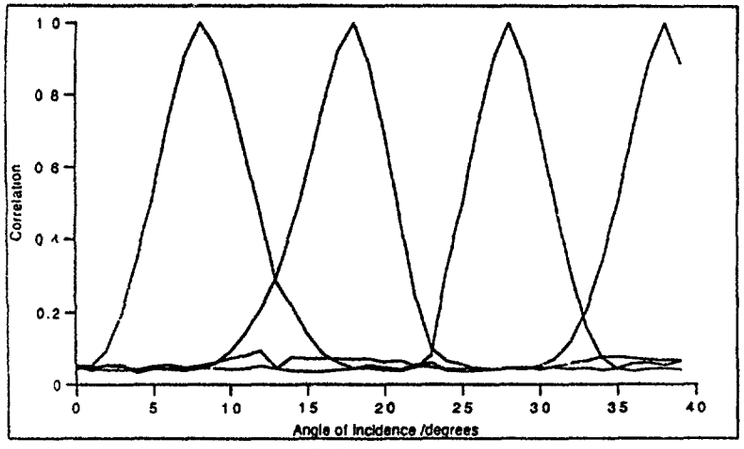

Surface B, RMS height 0.9 μm, Correlation Length 2.8 μm

The width of the curves decreases with increasing angle for this low-slope case.

The width of the curves is independant of angle for this high-slope case.

Waves in Random Media 3 (1991) S29–S39. Printed in the UK

Measurements of light scattering by a characterized random rough surface

J C Dainty, N C Bruce and A J Sant
Blackett Laboratory, Imperial College, London SW7 2BZ, UK

Received 26 November 1990

Abstract. Measurements are presented of the angular distribution of four wavelengths of light scattered by a one-dimensional random rough surface, whose probability density function is Gaussian with a standard deviation $\sigma = 1.22 \pm 0.02\,\mu$m and whose lateral correlation function is also Gaussian with $1/e$ width $\tau = 3.17 \pm 0.07\,\mu$m. The wavelengths used are 0.63, 1.15, 3.39 and 10.6 μm. The surface is used in two forms: coated with gold and as an almost lossless dielectric. The results are compared to those predicted by a double scattering form of the Kirchhoff formulation. Agreement is good at small angles of incidence but less good at larger angles of incidence.

1. Introduction

The experimental observation of enhanced backscattering from random rough surfaces of large root-mean-square slope, first reported by Mendez and O'Donnell [1,2], has stimulated a re-examination of the problem of light scattering in the past few years. The main progress to date has been the development of 'exact' numerical codes for the solution of Maxwell's equations from a one-dimensional surface illuminated with either s (i.e. TE) polarization or p (i.e. TM) polarization [3–7]. With s polarization, the electric vector is parallel to the grooves, whereas with p polarization it is perpendicular to the grooves, as in figure 1 (this figure also shows the sign convention used for the incident and scattering angles). An important feature of the work of Mendez and O'Donnell was that the surfaces were relatively well characterized, with Gaussian statistics for the surface height and a single-scale Gaussian correlation function. Since the statistics of the surface were known, a critical comparison between experiment and theory could be made with confidence.

The shape of the scattering cross section curves with angle of observation for high-sloped surfaces is quite different from that for simple low-sloped ones and early numerical results [3] were encouraging since they were in fairly good agreement with the experimental ones particularly at near-normal incidence. In order to carry out a more critical comparison between real experiments and numerical ones, it is important that the surface is well characterized and also helpful if a range of wavelengths are used. The results presented here are intended to supplement those already reported [8–10] with the aim of providing a reliable body of experimental data for comparison with numerical work and analytical theory. The surface used is one-dimensional, for two reasons: firstly, it can be characterized much more accurately than a two-dimensional one, since a sharp chisel-shaped stylus can be used in a surface profilometer; secondly,

0959-7171/91/03S029-11$03.50

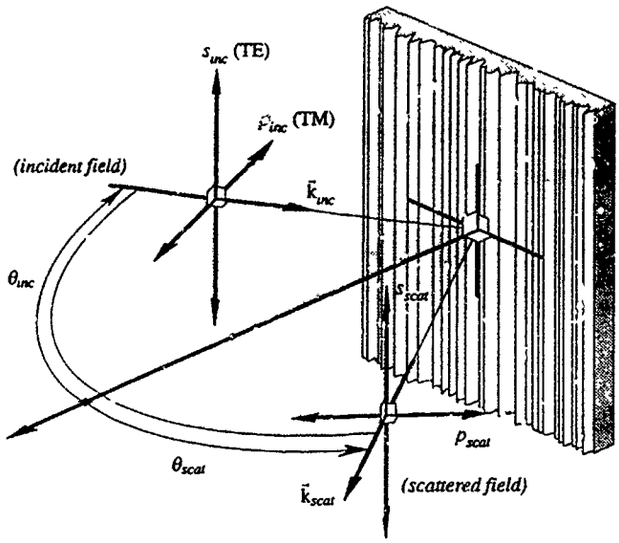

Figure 1. Polarization and angle notation for in-plane scattering from a one-dimensional rough surface

'exact' numerical calculations of the light scattering are only feasible at the present time for the one-dimensional case.

When comparing experimental measurements of light scattering with numerical computations, it is helpful if the numerical results provide some physical insight to the scattering process. For example, it is believed from the experiments that the mechanism giving rise to the enhanced backscatter peak is multiple scattering; however, numerical calculations based on exact theory do not separate the single and multiple scatter terms, and therefore do not provide the insight that is desirable (however, iterative solutions do separate the single and multiple scatter terms). For this reason, we have written numerical code based on a multiple (double and triple) scattering extension of the Kirchhoff boundary condition, including the effects of shadowing (see [11] for details and further references). In section 3 of this paper we compare the results of this code with the experimental results and 'exact' numerical code.

2. Experimental results

Master surfaces are produced by exposing a thick layer of photoresist ($\approx 12\,\mu$m of Shipley S1400-37) to several statistically independent laser speckle patterns. Two versions of the surface were prepared using a replication technique [8], one being coated with ≈ 1000 Å of gold and the other being an almost lossless dielectric of refractive index $n = 1.41$ (at $\lambda = 0.63\,\mu$m). Figure 2 shows the probability histogram of surface height and surface autocorrelation function, as measured by a Talystep profilometer whose stylus is a pyramid of 70° apex angle truncated by a flat region of $\approx 0.5\,\mu$m. Both are good fits to Gaussian functions, with the root-mean-square height $\sigma = 1.22 \pm 0.02\,\mu$m and $1/e$ correlation length $\tau = 3.17 \pm 0.07\,\mu$m. The angular distribution of the scattered

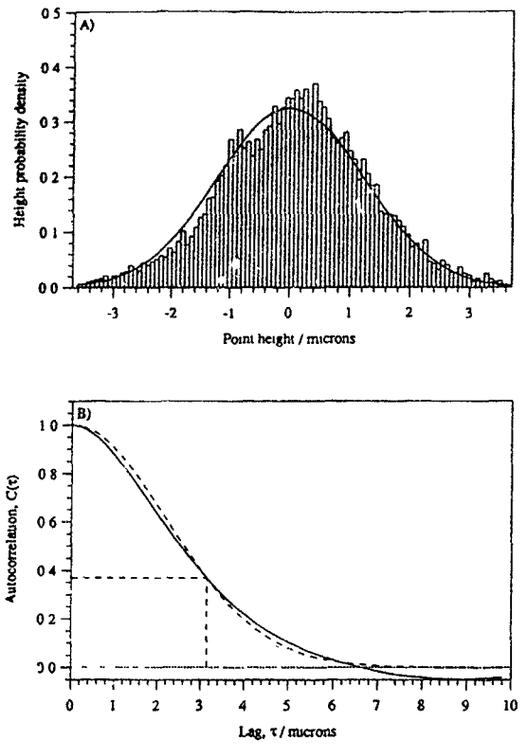

Figure 2. Probability histogram (upper) and autocorrelation function (lower) of the surface height fluctuation as calculated from Talystep measurements for the surface (#46) used in this paper.

light was measured at four wavelengths (0.63 μm, 1.15 μm, 3.39 μm and 10.6 μm) using the equipment described in [10]. For each angle of incidence, measurements are made with p-polarization incident and p-polarization collected ('p-p' scattering) and s-polarization incident and s-polarization collected ('s-s' scattering); no crossed polarized components were detectable. For a perfect conductor, these measurements give a complete description of the scattering characteristics of the surface, but in general four scattering coefficients are required for materials of finite conductivity; these can be found by measuring the polarization of the scattered light for various input polarizations. Also, the measurements reported here yield the relative scattering cross section, as no absolute calibration is performed.

The relative scattering cross sections for angles of incidence of 0°, −30° and −60° and the four wavelengths are shown in figures 3 and 4 for the gold-coated surface and figures 5 and 6 for the dielectric surface. The enhanced backscatter peak, where present, occurs on the right-hand side of the graphs (i.e. at positive angles, see figure 1 for the sign convention for the angles) and any specular component is on the left-hand side (i.e. negative angles); for the 10.6 μm measurements, the specular peak was very much greater than the diffuse component and is not shown. A few features are of particular note.

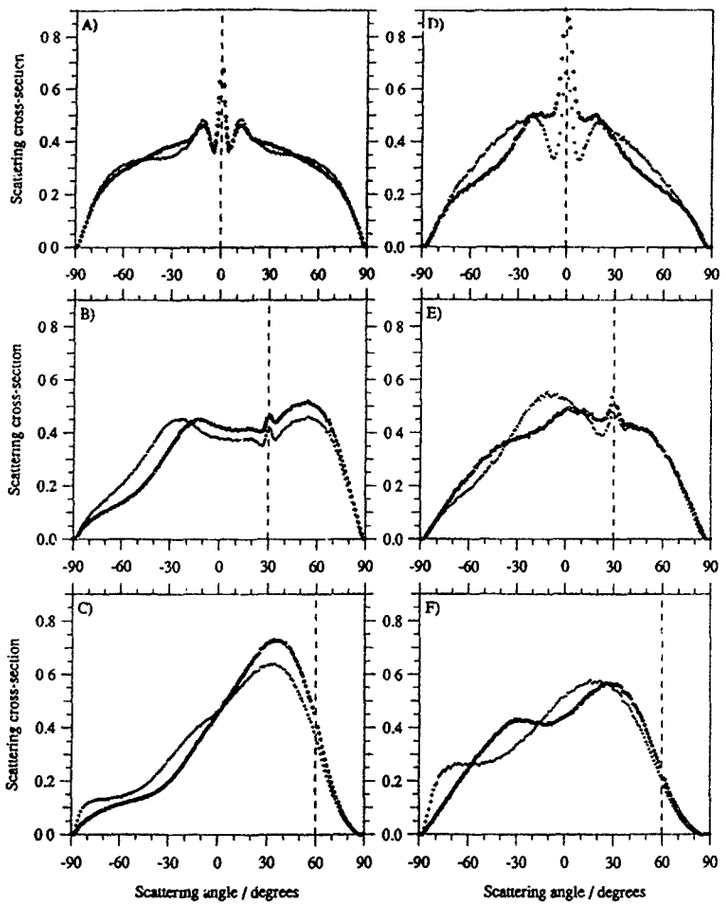

Figure 3. Relative scattering cross section as a function of scattering angle for the gold-coated surface, for angles of incidence of 0°, −30° and −60°, for p-p scattering (open circles) and s-s scattering (crosses). The left-hand column is for a wavelength of 0.63 μm, for which $\sigma/\lambda = 1.93$ and $\tau/\lambda = 5.02$ and the right-hand column for $\lambda = 1.15\,\mu$m, for which $\sigma/\lambda = 1.07$ and $\tau/\lambda = 2.76$. The enhanced backscatter peak, where present, occurs at positive angles (right-hand side of each graph).

(1) The enhanced backscatter peak and sidelobe structure are clearly visible for the shorter wavelengths at an angle of incidence less than approximately −30° for the gold-coated surface; the width of the peak is proportional to the wavelength. The peak is not observed for the p-p scattering at 10.6 μm for the gold surface or for scattering from the dielectric.

(2) With the exception of the p-p case at 10.6 μm, the p-p and s-s scattering by the gold surface are very similar; for the dielectric surface, however, the p-p and s-s scattering cross sections are quite different, as one might expect by analogy with reflection from a planar surface. Using a value of $n = 1.41$ for the refractive index of the (almost lossless)

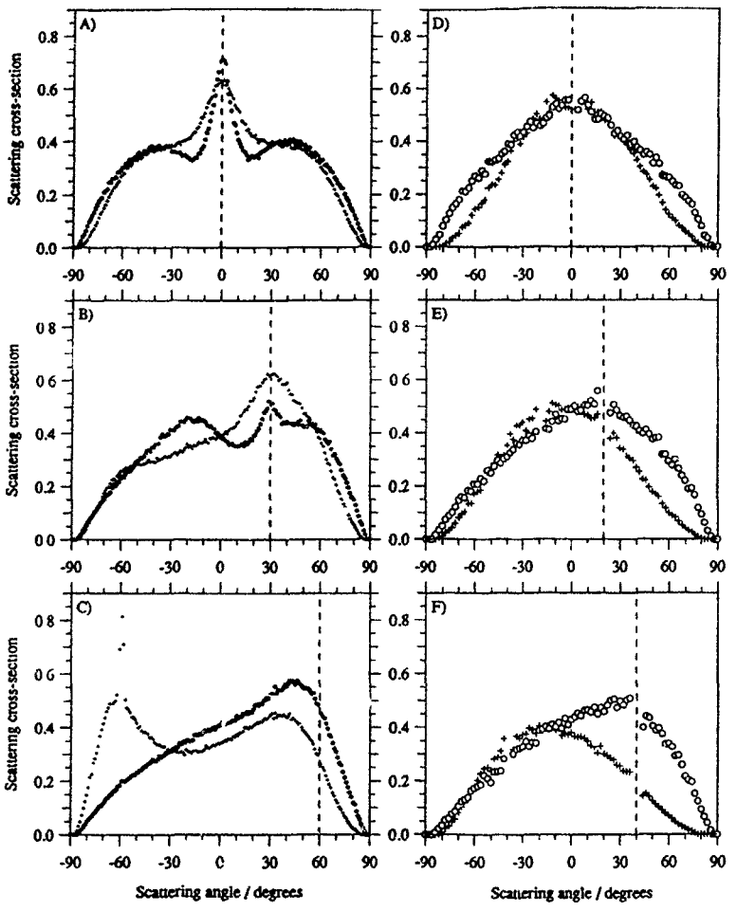

Figure 4. As for figure 3 but wavelengths of 3.39 μm ($\sigma/\lambda = 0.36$, $\tau/\lambda = 0.94$) and 10.6 μm ($\sigma/\lambda = 0.12$, $\tau/\lambda = 0.30$). For the 10.6 μm curves, the angles of incidence were 0°, −20° and −40°. The (strong) specular component in the 10.6 μm curves is not shown

dielectric gives a Brewster angle of ≈ 55°. Considering single scattering to be the dominant mechanism and treating this as a reflection from a locally plane surface gives an expected minimum of the p-p scattered intensity at an angle equal to approximately (−110° − incident angle): the angles are roughly in accordance with this simple picture. The s-s and p-p scattered intensities in the backscatter direction appear to be almost equal to each other for all angles of incidence and wavelengths, for the dielectric.

(3) The overall shape of the curves is dramatically different from the Gaussian-type shapes (centred on the specular angle) normally encountered in scattering from low-sloped surfaces.

The principal purpose of figures 3 to 6 is to provide a reliable set of data for comparison with numerical calculations, and analytical theories should any become available.

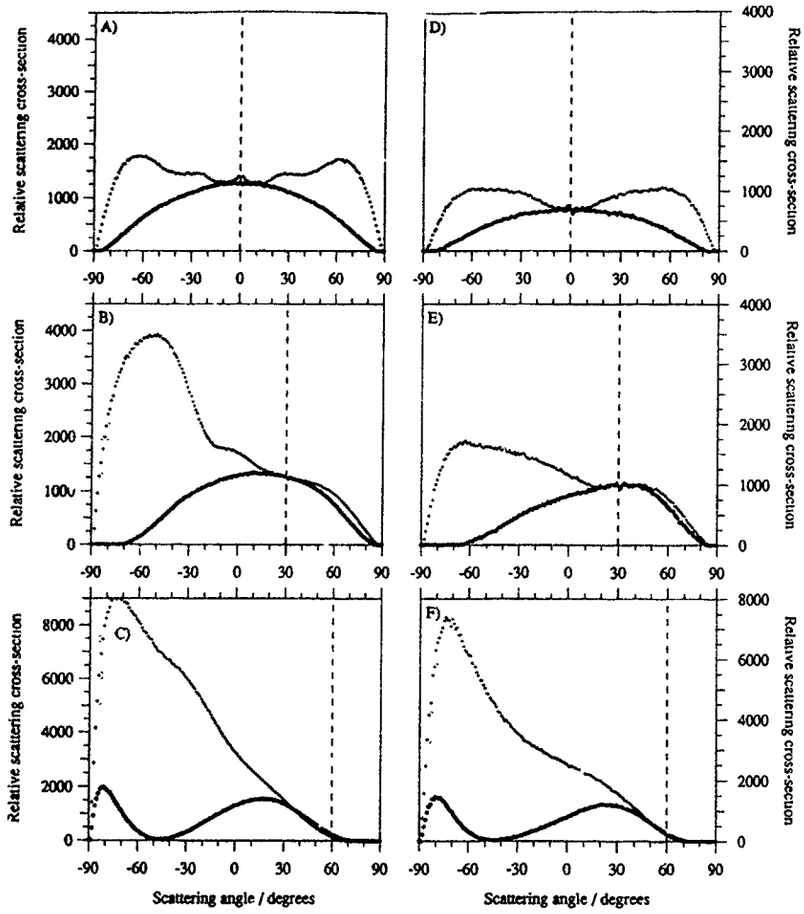

Figure 5. As for figure 3 but for the dielectric surface, $n_{0.63} = 1.41$, $n_{1.15} = 1.40$. The vertical scale is not the same as that used in figure 3 (both are *relative* scattering cross sections).

3. Kirchhoff multiple scatter approximation

One can compare the above experimental results to those of 'exact' numerical calculations based on the extinction theorem and its extensions [3–7], and some comparisons of experiment and calculations for a perfect conductor were given in [10]. Although such comparisons are valuable, one problem with the 'exact' numerical solution is that it gives little physical insight into the problem. We have therefore attempted to extend the Kirchhoff approximation (i.e. tangent plane approximation for each scattering event) to double (and multiple) scattering [11].

The numerical calculations were carried out using the method described in [11] for a perfect conductor; typically the energy conservation (unitarity) held to better than 3% considering just the single and double scatter terms for surface #46 (except for the

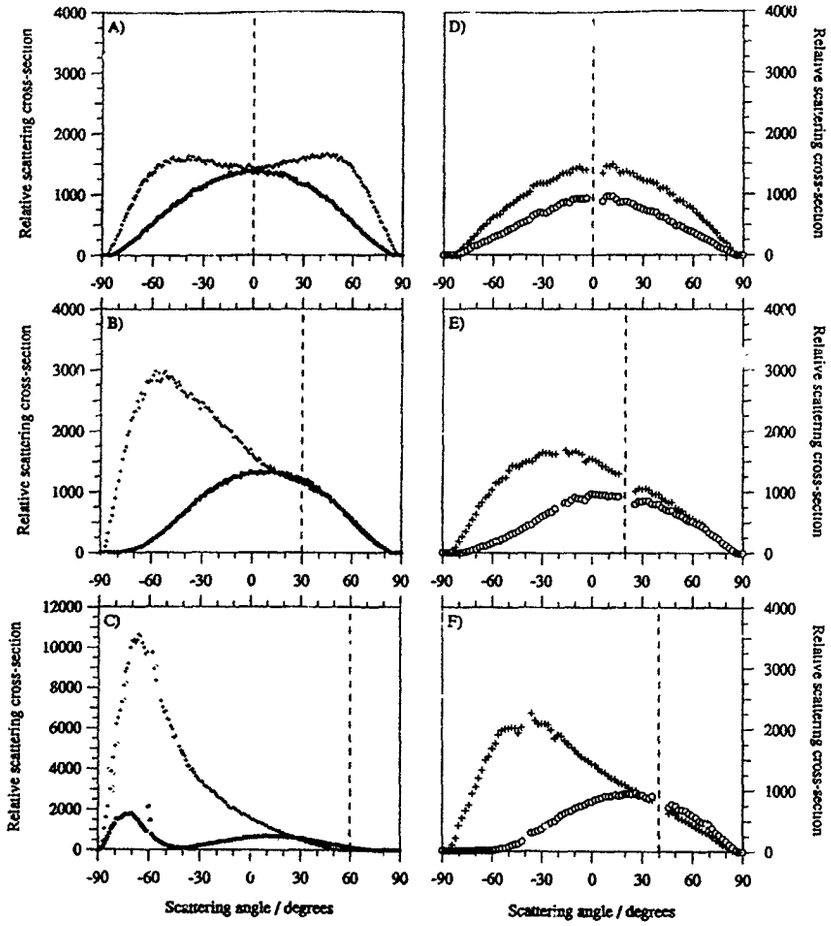

Figure 6. As for figure 4 but for the dielectric surface, $n_{3.39} = n_{10.6} = 1.41$.

$-60°$ results for which the departure from unitarity is $\approx 6\%$) and the results are averaged over approximately 10^3 realizations. Figures 7 and 8 show the results of the calculations for $\lambda = 0.63\ \mu$m and $1.15\ \mu$m respectively, for incident angles of $0°$, $-30°$ and $-60°$ and s-s and p-p scattering. Each graph shows the single, double and total scattered intensity. The enhanced backscatter peak occurs *only* in the double scatter component, showing conclusively that the enhancement is a multiple scattering effect. The enhancement is on the order of a factor of two in the double scattered component for all angles of incidence, but the enhancement in the total intensity is much less than two and decreases with increasing angle of incidence due to the fact that the double scattered intensity also decreases with incidence angle.

Figure 9 compares the total scattered intensity for s-s scattering from figures 7 and 8 with the results of 'exact' numerical calculations (based on the extinction theorem method for a perfect conductor [3]) and the experimental results of figure 3, for

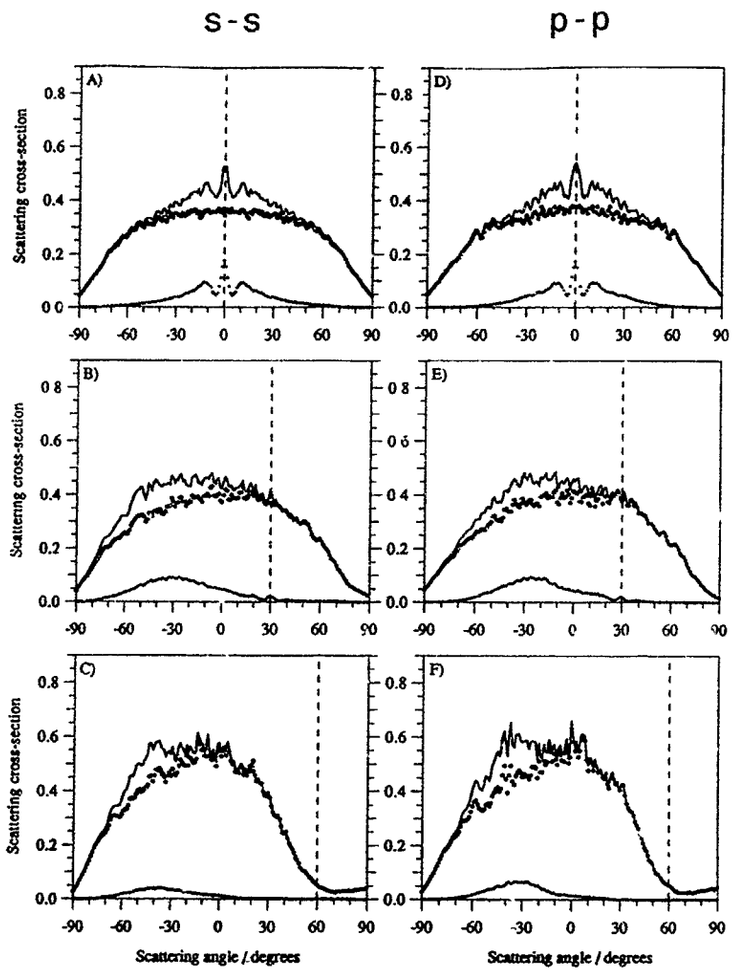

Figure 7. Numerically calculated scattered intensities for a perfect conductor, using the double-scattering Kirchhoff approximation, for angles of incidence of 0°, −30° and −60° and s-s scattering (left) and p-p scattering (right). The wavelength is 0.63 μm. Each graph shows the doubly scattered intensity (lowest curve), single scattered (middle) and total intensity (coherent sum) (top curve).

$\lambda = 0.63\ \mu$m and 1.15 μm at three angles of incidence. The two numerical calculations agree well, showing that the Kirchhoff approximation is reasonable for these surface parameters (the average radius of curvature, defined as the inverse of the standard deviation of the surface curvature $2\sqrt{3}\sigma/\tau^2$, is $\approx 2.4\ \mu$m for surface #46) and both agree well with the experimental measurements for zero angle of incidence. However, there is a clear discrepancy between experiment and numerical calculation for the −30° and −60° angles of incidence. (This general behaviour is also shown in the case of *p-p* scattering.)

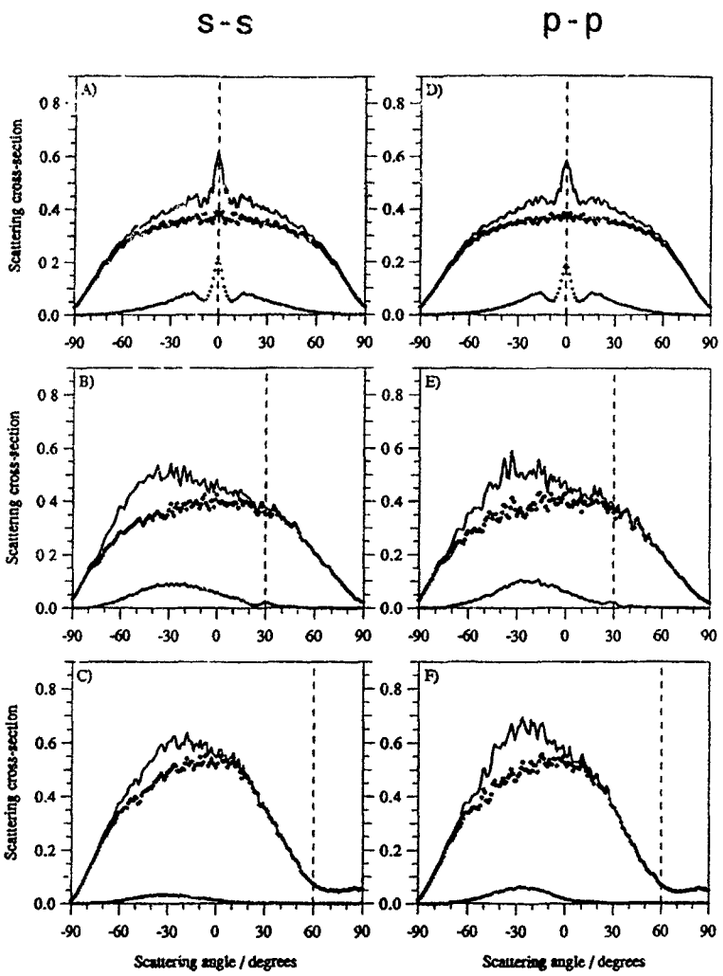

Figure 8. As for figure 7, but wavelength of 1.15 μm.

One possible cause of the discrepancy could be that the calculations are for a perfect conductor, whereas the experiments are for a real metal (gold). However, calculations by ourselves and others [5] show that, for these values of RMS surface height and correlation length, there is very little difference between the results for gold and for a perfect conductor, particularly for s-s scattering. One problem with most methods of calculation, including that used here, is that a very small length of surface is considered, giving rise to the possibility of an 'end-effect' error (e.g. due to long-range surface plasmons); however, the method of calculation of Saillard and Maystre [7] uses an extremely long length of surface with good agreement with the other calculations and poor agreement with the measurements at larger angles of incidence.

It seems, therefore, that there may be some aspect of the experiment that does not correspond to the calculations. Previous results for a Lambertian diffuser have

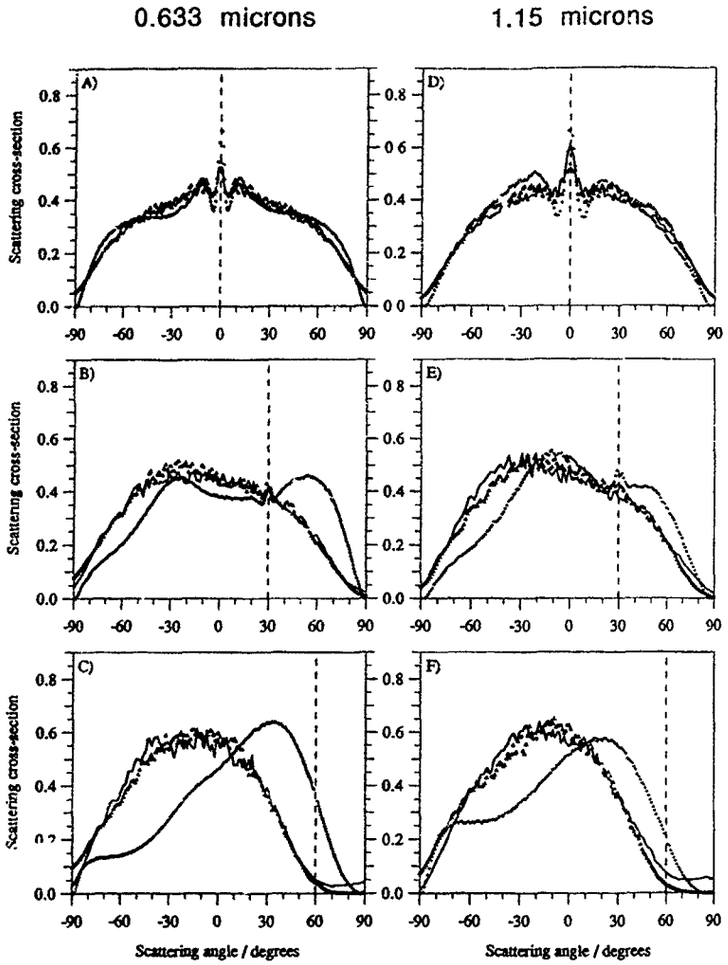

Figure 9. Comparison of Kirchhoff calculation (from figures 7 and 8), 'exact' numerical calculation and experiment (from figure 3), for *s-s* scattering at $\lambda = 0.63\,\mu$m and $1.15\,\mu$m, and angles of incidence equal to 0°, −30° and −60°. The solid curves are the Kirchhoff calculation, triangles the 'exact' calculation and crosses are the experimental results. Note the good agreement between the two numerical calculations but the departure of the experimental results for larger angles of incidence.

demonstrated that the scatterometer measures the correct quantity [10]. The measurement of surface properties might be in error. If one calculates the scattered intensity for, say, −60° angle of incidence for a surface that has an RMS roughness 50% larger than the measured value, then reasonable agreement is obtained between experiment and numerical calculation. However, (*a*) it is extremely unlikely that such a gross error could occur (stylus tips effects are discussed by Church [12]) and (*b*) the agreement for 0° angle of incidence is then very poor indeed, particularly as regards the location of the minima around the backscatter peak. Ishimaru and Chen [13] have shown that

a departure from Gaussianity of the correlation function could be responsible for the discrepancy, and the measured correlation does show a small departure from the Gaussian shape. However, it is notoriously difficult to estimate the correlation function of stylus traces and the departure shown in figure 2 is characteristic of inadequate de-trending of the mean; the method of manufacture of the surfaces strongly encourages a Gaussian correlation of surface height. The cause of this discrepancy for larger angles of incidence is therefore not resolved at the present time.

4. Summary

A set of scattering data for a one-dimensional surface at four wavelengths, three angles of incidence and two materials has been presented for critical comparison with numerical calculations and theoretical studies. A multiple scatter extension of the Kirchhoff approximation has been shown to provide additional physical evidence that the predominant cause of the enhanced backscatter peak is due to multiple scattering. There remains a significant disagreement between experiment and numerical calculations for large angles of incidence the cause of which is still unresolved.

The data presented in figures 3 to 6, together with sample Talystep traces, is available on a PC- or Macintosh-compatible diskette on application to the first author.

Acknowledgments

This work is supported by the UK Science and Engineering Research Council (GR/F81651) and the US Army (DAJA45-90-C-0026). JCD is also grateful to A A Maradudin and M Nieto-Vesperinas for discussions made possible by a Nato Travel Grant (890528).

References

[1] Mendez E R and O'Donnell K A 1987 *Opt Commun.* **61** 91–5
[2] O'Donnell K A and Mendez E R 1987 *J. Opt. Soc. Am* A **4** 1194–205
[3] Nieto-Vesperinas M and Soto-Crespo J-M 1987 *Opt. Lett.* **12** 979–81
[4] Maradudin A A, Mendez E R and Michel T 1989 *Opt Lett.* **14** 151–3
[5] Maradudin A A, Michel T, McGurn A R and Mendez E R 1990 *Ann. Phys.* **203** 255–307
[6] Thorsos E I 1988 *J. Acoust. Soc. Am.* **83** 78–92
[7] Saillard M and Maystre D 1990 *J. Opt. Soc. Am.* A **7**, 982–90
[8] Sant A J, Kim M-J and Dainty J C 1989 *Opt. Lett.* **14** 1183–5
[9] Dainty J C, Kim M-J and Sant A J 1990 *Scattering in Surfaces and Volumes* (Amsterdam: Elsevier) pp 143–55
[10] Kim M-J, Dainty J C, Friberg A T and Sant A J 1990 *J. Opt. Soc. Am.* A **7** 569–77
[11] Bruce N C and Dainty J C 1991 *J. Mod. Opt.* **38** 579–90
[12] Church E 1990 *Paper* presented at Conf. on Modern Analysis of Scattering Phenomenon, Marseille, September, 1990
[13] Ishimaru A and Chen J S 1991 *Opt. Lett.* in press

Optics Communications 88 (1992) 471–484
North-Holland

OPTICS
COMMUNICATIONS

Full length article

The Mueller matrix for rough surface scattering using the Kirchhoff approximation

N.C. Bruce, A.J. Sant and J.C. Dainty
Blackett Laboratory, Imperial College, London SW7 2BZ, UK

Received 7 August 1991

The Kirchhoff approximation is used to find the scattered intensities and the Mueller matrix for a gaussian surface with standard deviation of height $\sigma = 1.22$ μm and correlation length $\tau = 3.18$ μm using a wavelength of $\lambda = 0.633$ μm. The cases of gold ($n = 0.167 + i\,3.149$) and dielectric ($n = 1.41$) surfaces are considered. Results are compared with experimental observations and are shown to give good agreement. The single and double scattered intensities are shown to be fully polarised for both cases whereas the total (single plus double) shows a strong unpolarised component for the gold case. This effect is understood by considering that the single and double scatter terms are partially coherent and at right angles to each other.

1. Introduction

Scattering of electromagnetic waves from one-dimensional rough surfaces has been a topic of much interest in recent years, the motivation for a great deal of this work being the phenomenon of enhanced backscatter [1,2]. Experimental [3–5] and theoretical [6–10] curves for the distribution of scattered intensity for the two cases of s-polarisation (TE) incident and scattered (denoted by ss) and p-polarisation (TM) incident and scattered (denoted by pp) have been found. These cases have been considered, since for a one-dimensional surface (i.e. a surface for which the height is constant in one direction) there is no scattering from s to p or from p to s; s and p are the two fundamental polarisations into which all other polarised cases can be decomposed. However, as has been pointed out recently [5], the ss and pp intensity distributions do not give a full representation of the scattering process for these surfaces. This is due to the fact that the relative phase of the ss and pp scattered fields is not contained in the ss and pp intensities. For example an incident field polarised at 45° to the plane of incidence may give a component of the scattered field circularly polarised (i.e. an incident field with s and p components the same amplitude and in phase could give a scattered field with s and p the same amplitude with a $\pi/2$ phase difference). In the ss and pp intensities these phase terms are not used since the modulus squared of the scattered field is calculated.

In calculations of the intensity distribution the scattered field is first evaluated and the modulus square then taken. This means that the phase term can be found directly from the calculations. However, in experiments only the intensity can be measured so the phase difference cannot be directly found. Instead the scattered intensities for certain combinations of incident and detected polarisations are required to find the Stokes parameters of the scattered light [11].

In this communication the recently developed multiple scattering Kirchhoff approximation (KA) [12–16] is used to calculate the Stokes parameters for a particular surface. The advantage of the KA is that the single and double scatter terms can be separated i.e. it is possible to separate light paths intersecting the surface profile once or twice. The calculation has been performed for a gold surface with refractive index $n = 0.167 + i3.149$ (at $\lambda = 0.633$ μm) and a dielectric surface of $n = 1.41$.

The theory of the calculations and experimental procedure is discussed in sect. 2 and comparisons of

numerical and experimental results are given in sect. 3.

2. Theory

In the Kirchhoff approximation the total field on the surface is approximated by the incident field plus the reflected field at each point. The reflection is assumed to be from a plane to permit Fresnel reflection coefficients to be used. This gives a condition for the approximation to be valid – the radius of curvature at each point of the surface must be large compared to the illuminating wavelength. The single scatter term is given by [12,13]

$$E_s^{[1]}(\theta)=-\left(\frac{2}{\pi kr}\right)^{1/2}\frac{\exp(i\varphi)}{2}\,\frac{1+\cos(\theta+\theta_i)}{\cos\theta+\cos\theta_i}\times\int_\Gamma S(x',z')R\exp[i(k_i-k)\cdot R]\,dx', \tag{1}$$

where θ_i and θ are the incident and scatter angles respectively, φ is a phase term independent of x', R is the position vector of the point (x', z'), R is the planar reflectivity for the tangent at (x', z') and $S(z', z')$ is a shadow function depending on both θ_i and θ. The double scatter contribution can be considered as two terms, first the field at any surface point due to light from one other surface point is

$$E_s(x_2,z_2)=-\frac{1}{4i}S_{12}\left\{(1+R_1)\left[m_1\frac{k(x_2-x_1)}{r_{12}}-\frac{k(z_2-z_1)}{r_{12}}\right]H_1^{(1)}(kr_{12})-(1-R_1)ik(m_1\sin\theta_i+\cos\theta_i)H_0^{(1)}(kr_{12})\right\}E_i(x_1,z_1), \tag{2}$$

with S_{12} a shadow function depending on θ_i and the vector between points 1 and 2, m_1 the gradient of the surface at the first point, R_1 the Fresnel reflection coefficient at the first point and $H_0^{(1)}(kr_{12})$ and $H_1^{(1)}(kr_{12})$ the zeroth and first order Hankel functions of the first kind. The total field due to all combinations of first and second points is

$$E_s^{[2]}(\theta)=-\left(\frac{2}{\pi kr}\right)^{1/2}\frac{\exp(i\varphi)}{4}\int_\Gamma\int_\Gamma S'\Big[(1+R_2)\times k(m_2\sin\theta-\cos\theta)E_s(x_2,z_2)+i(1-R_2)\frac{\partial E_s(x_2,z_2)}{\partial n_2}\Big]\exp(ik\cdot R_2)\,dx_1\,dx_2, \tag{3}$$

where S' represents the shadow function for the scattered radiation, m_2 is the gradient of the surface at the second point and R_2 is the Fresnel reflection coefficient at the second surface point. The shadow functions used here are geometric (straight line) shadow functions and were calculated explicitly for every point (or combination of points) by performing a ray trace. If the ray of interest was intersected by the surface at any point the shadow function took the value zero and the contribution from that point was neglected. Eqs. (2) and (3) together represent the double scatter contribution. Any material dependence is entirely contained within the Fresnel reflectivity coefficients R, R_1 and R_2. Light paths traversing inside the material are not included in this method but it is expected that the contribution from such paths is small since the necessary scatter angles are large compared to the refraction angles of the materials considered. The simplest case occurs for a perfect conductor for which $R=1$ for p-polarisation and $R=-1$ for s causing most of the above terms to drop out, leaving only one contribution for each case. Eqs. (1), (2) and (3) are discretised and programmed into a computer. Intensity curves are calculated for particular surface profiles and the intensities averaged over typically 800 different surfaces of the same statistics to produce the final curves.

The convergence of the series given by the sum of the Kirchhoff single scatter plus double scatter plus etc. has not been proved rigorously. However, calculations of the triple scatter term show that the integrated energy in this order of scattering is much smaller than in the double scatter (approximately 1/50th the double scatter). While this does not prove the convergence of the series, it at least shows a required effect – the relative importance of the results of higher order calculations should decrease as the order increases.

The scattering of the field can be denoted in matrix terms as

$$\begin{pmatrix}E_p\\E_s\end{pmatrix}=\begin{pmatrix}f_{pp}&0\\0&f_{ss}\end{pmatrix}\begin{pmatrix}E_{ip}\\E_{is}\end{pmatrix}, \tag{4}$$

where E_p and E_s are the scattered p and s fields, E_{ip} and E_{is} are the incident p and s fields and f_{pp} and f_{ss} are the field scattering coefficients. This can be written since any polarised state can be decomposed into s and p components and there is no depolarisation for scattering of s and p from one-dimensional surfaces. Note that all the terms represent complex numbers and are functions of angles. The Stokes vector is given by four parameters which give for the scattered wave [11]

$$I=\langle E_pE_p^*+E_sE_s^*\rangle, \quad Q=\langle E_pE_p^*-E_sE_s^*\rangle,$$
$$U=\langle E_pE_s^*+E_sE_p^*\rangle, \quad V=\mathrm{i}\langle E_pE_s^*-E_sE_p^*\rangle, \tag{5}$$

where $\langle\ \rangle$ denotes the average over different surfaces of the same statistics. These give a full characterisation of the polarisation properties of the scattered wave.

The Stokes parameters of the scattered field are related to those of the incident field by the Mueller matrix, M

$$S=MS_0, \tag{6}$$

where M is a 4×4 matrix which, for the one-dimensional case is given by

$$M=\begin{pmatrix} m_{11} & m_{12} & 0 & 0 \\ m_{12} & m_{11} & 0 & 0 \\ 0 & 0 & m_{33} & m_{34} \\ 0 & 0 & -m_{34} & m_{33} \end{pmatrix}. \tag{7}$$

This matrix describes fully the scattering properties of the target surface. For an incident polarisation at $+45°$ (halfway between the s and p polarisation directions) the incident Stokes vector is

$$S_0=\begin{pmatrix} 1 \\ 0 \\ 1 \\ 0 \end{pmatrix}, \tag{8}$$

so that the final Stokes vector of the scattered light is, from eq. (6)

$$S=\begin{pmatrix} m_{11} \\ m_{12} \\ m_{33} \\ -m_{34} \end{pmatrix}, \tag{9}$$

i.e. the final Stokes vector is just given by the separate non-zero Mueller matrix elements. In the calculations E_{ip} and E_{is} are set to $1/\sqrt{2}$ to give an incident unit amplitude plane wave linearly polarised at $+45°$. The scattered s and p fields are found from eqs. (1) to (3) and the Stokes matrix, and hence the Mueller elements, are found by using eq. (5).

Experimentally the Mueller matrix elements are found by measuring the scattered intensity distribution using suitable combinations of incident and detected polarisations [5,11,14]. The terms m_{11} and m_{12} are measured by using p-polarisation incident and p detected (given by I_p) and s incident and s detected (I_s). The signals resulting are added for m_{11} and subtracted (p-polarised − s-polarised) for m_{12}. m_{33} is found by scattering light polarised at $+45°$ then finding the difference of the scattered light polarised at $+45°$ (I_+) minus that polarised at $-45°$ (I_-). The final term is found by again using incident light polarised at $+45°$ and finding the difference of left circularly scattered light (I_L) minus right circularly scattered light (I_R) [17].

The four Stokes parameters obey the following relation [18,19]

$$I^2\geqslant Q^2+U^2+V^2, \tag{10}$$

the equality holding for fully polarised light. For the case of incident polarisation at $+45°$ the terms of this expression are given by eq. (9). It is thus possible to separate the polarised and unpolarised components of the scattered energy for this situation, the polarised being given by $(Q^2+U^2+V^2)^{1/2}$ and the unpolarised by $I-(Q^2+U^2+V^2)^{1/2}$.

3. Results

The validity of using the Kirchhoff approximation is limited to surfaces containing radii of curvature greater than the illuminating wavelength to permit the use of *planar* reflection coefficients in eqs. (1), (2) and (3). The applicability of the method to the surface used can be verified by noting that the radius of curvature is approximately the inverse of the second derivative of the surface profile. As the height distribution is gaussian so is the second derivative with a standard deviation $\sigma_{h''}$ given by

$$\sigma_{h''} = 2\sqrt{3}(\sigma_h/\tau^2)\,, \qquad (11)$$

where σ_h is the standard deviation of the gaussian probability distribution of heights and τ is the 1/e level of the gaussian autocorrelation function for the surface of interest. This gives a value of $\sigma_{h''} = 0.42$ μm^{-1} for the case considered here (surface #46 with $\sigma = 1.22$ μm and $\tau = 3.18$ μm). Therefore, approximately 67% of the radii of curvature will have values greater than 2.4 μm, so most of the curvatures have values greater than the wavelength leading to the conclusion that it is reasonable to expect the Kirchhoff approximation to be valid in this case.

The calculated unitarity or relative scattered energy for the gold and dielectric surfaces are given in table 1 for the single, double and total (single plus double added coherently) components of the fundamental polarisations s and p. The values of total scattered energy for these surfaces are less than one due to the finite conductivity of the surface materials causing light to be transmitted or absorbed.

Figs. 1 and 2 show the Kirchhoff single and double scatter terms for the gold and dielectric cases respectively. Note that there are different scales on the single and double graphs for both situations. The vertical dashed line on the graphs marks the incident direction so that light scattered in this direction is backscattered. Enhanced backscatter effects can be seen in the double scatter terms only, as expected from previous work [12–16]. In the gold case the m_{12} term is very small for both single and double which means that there is very little difference between the s and p scattered intensities. In the dielectric curves this difference is more important, as expected, since the Fresnel reflection coefficients show a bigger difference for a dielectric than for a good conductor.

The total (single and double) scattered intensities are shown in figs. 3 and 4 for the gold and dielectric cases respectively and are compared with the experimentally measured values. In the gold case the agreement is reasonably good at low angles of incidence apart from the m_{34} term which is much smaller in the calculations. As in other measurements [8,12] the agreement at higher angles of incidence is not so good; this appears to be the case for all methods of calculation, not just the Kirchhoff method. The reason for the difference in the m_{34} term, which is the difference between right and left circularly polarised light, may be that the refractive index of the material is not exactly as used in the calculation so that the phase difference between the s and p scattered components is different to that expected. The agreement for the dielectric case is much better. Since the refractive index is real for this material there is no scattering from linear to circular polarisation so m_{34} is near zero in this case.

The degree of polarisation of the scattered light is illustrated in figs. 5 and 6 for the calculations of the single and double scatter terms and figs. 7 and 8 for

Table 1
Gold surface

Incidence	s-polarisation			p-polarisation		
	single	double	total	single	double	total
0°	0.871	0.085	0.943	0.869	0.078	0.925
20°	0.861	0.010	0.949	0.859	0.084	0.911
40°	0.874	0.076	0.904	0.869	0.078	0.920

Dielectric surface

Incidence	s-polarisation			p-polarization		
	single	double	total	single	double	total
0°	0.033	0.0008	0.033	0.021	0.00004	0.020
20°	0.035	0.0017	0.036	0.019	0.00006	0.019
40°	0.045	0.003	0.045	0.017	0.0001	0.017

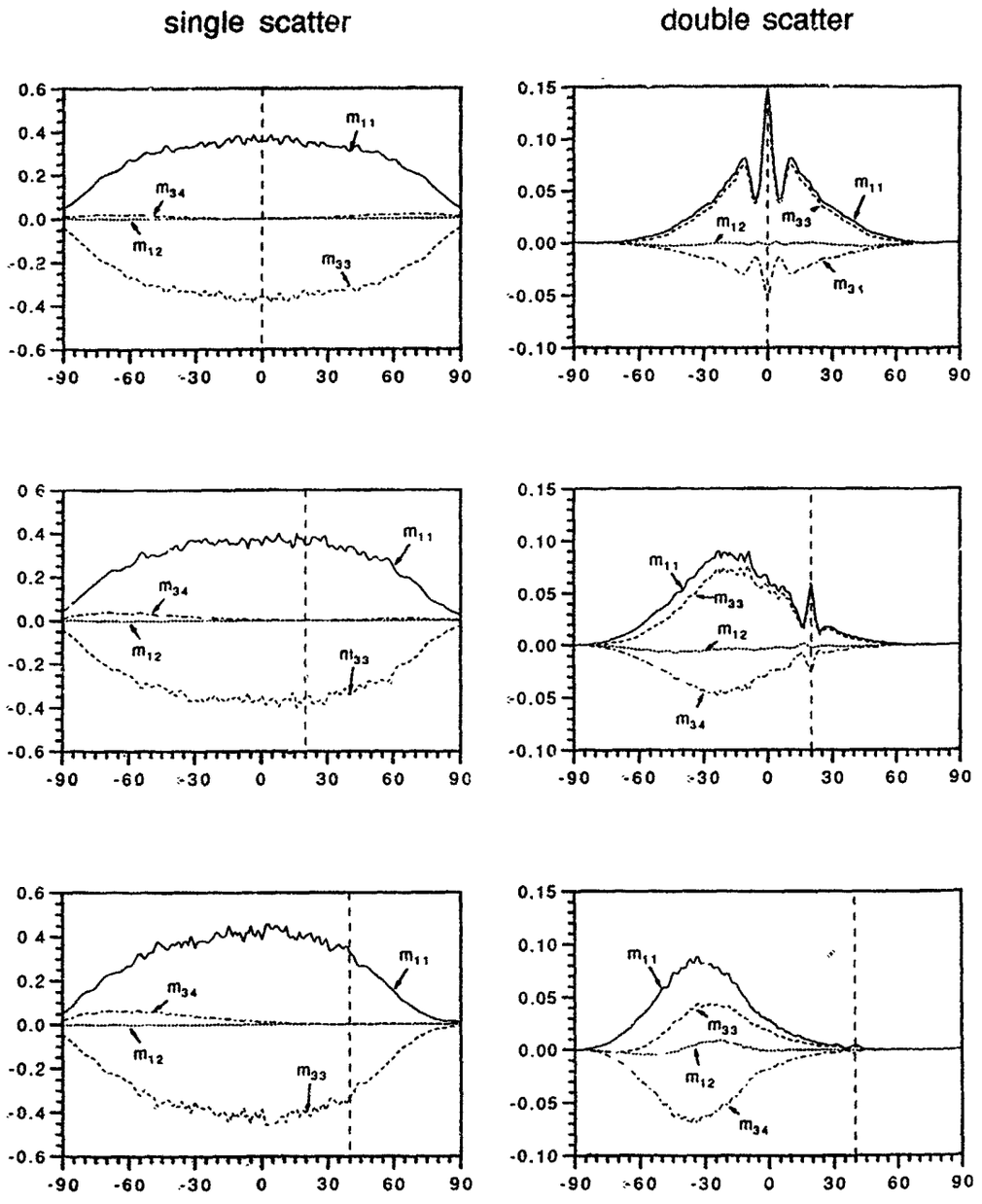

Fig. 1. Graphs of Mueller matrix terms (m_{11}, m_{12}, m_{33}, m_{34}) as a function of scatter angle for 0° incidence (top), 20° incidence (middle) and 40° incidence (bottom). Single scatter (left) and double scatter (right) for gold coated surface #46

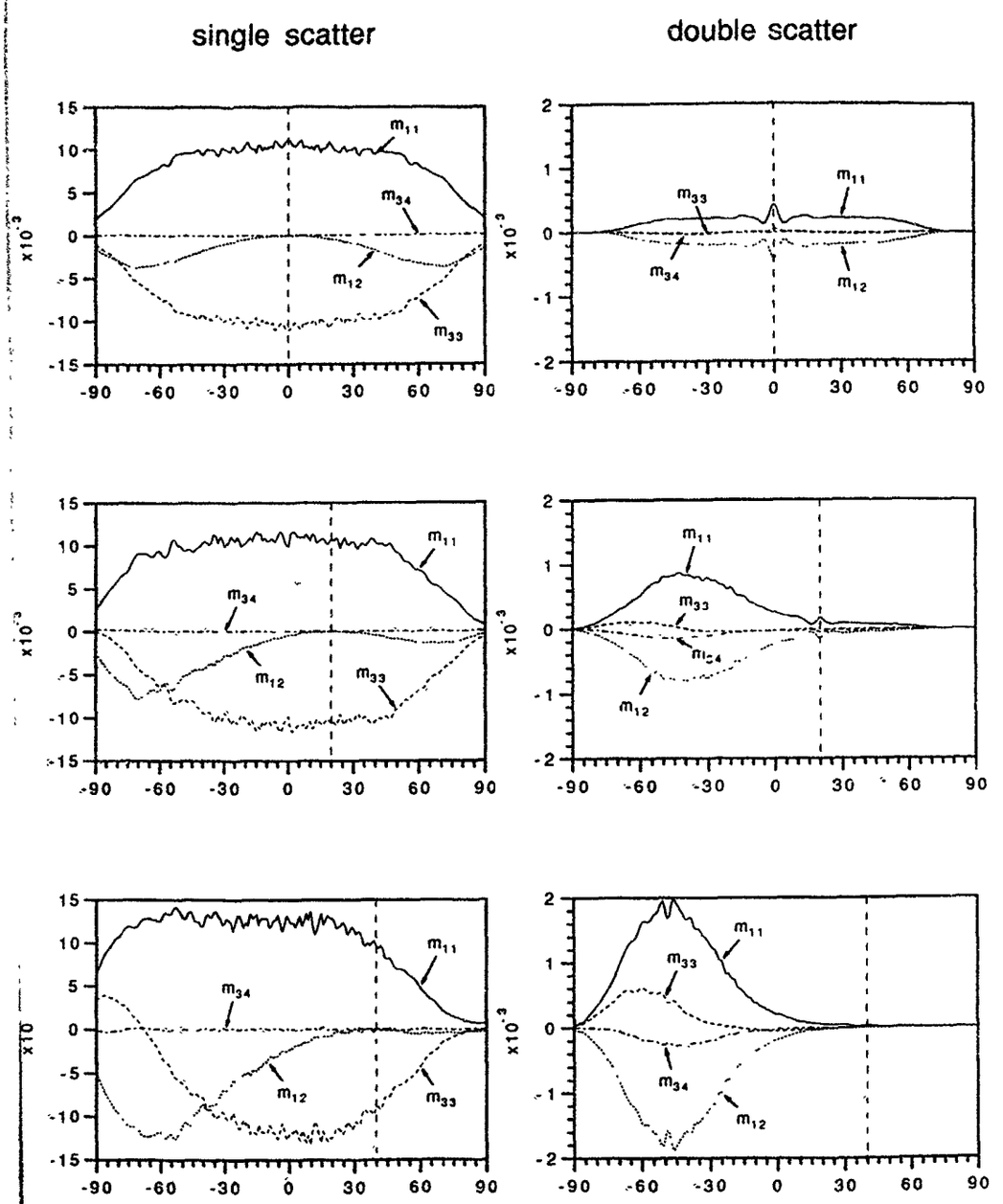

Fig. 2. As fig. 1 but for the case of dielectric surface #46.

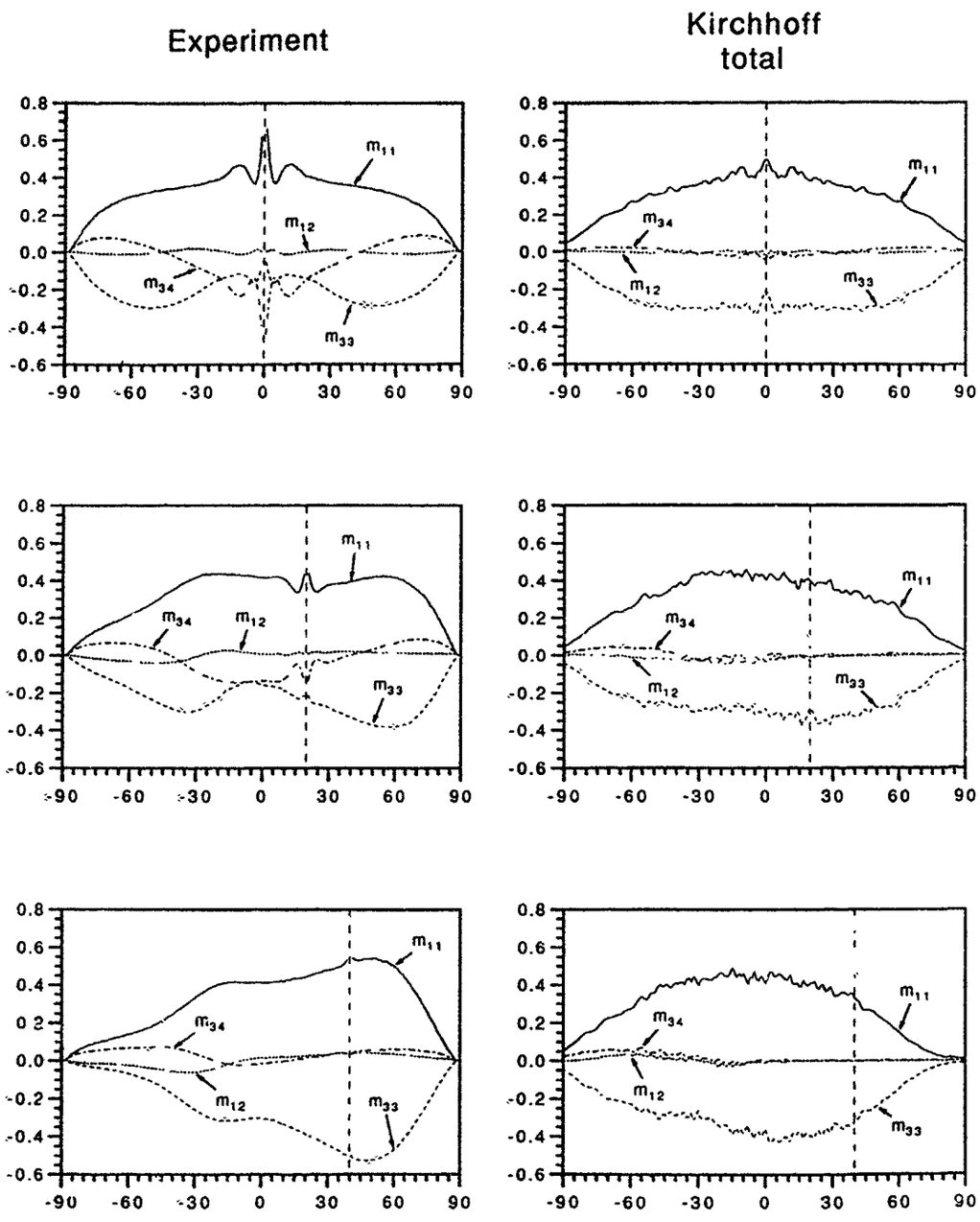

Fig. 3. Graphs of Mueller matrix terms ($m_{11}, m_{12}, m_{33}, m_{34}$) as a function of scatter angle for 0° incidence (top), 20° incidence (middle) and 40° incidence (bottom). Experimental results (left) and Kirchhoff total (single+double) (right) for gold coated surface #46.

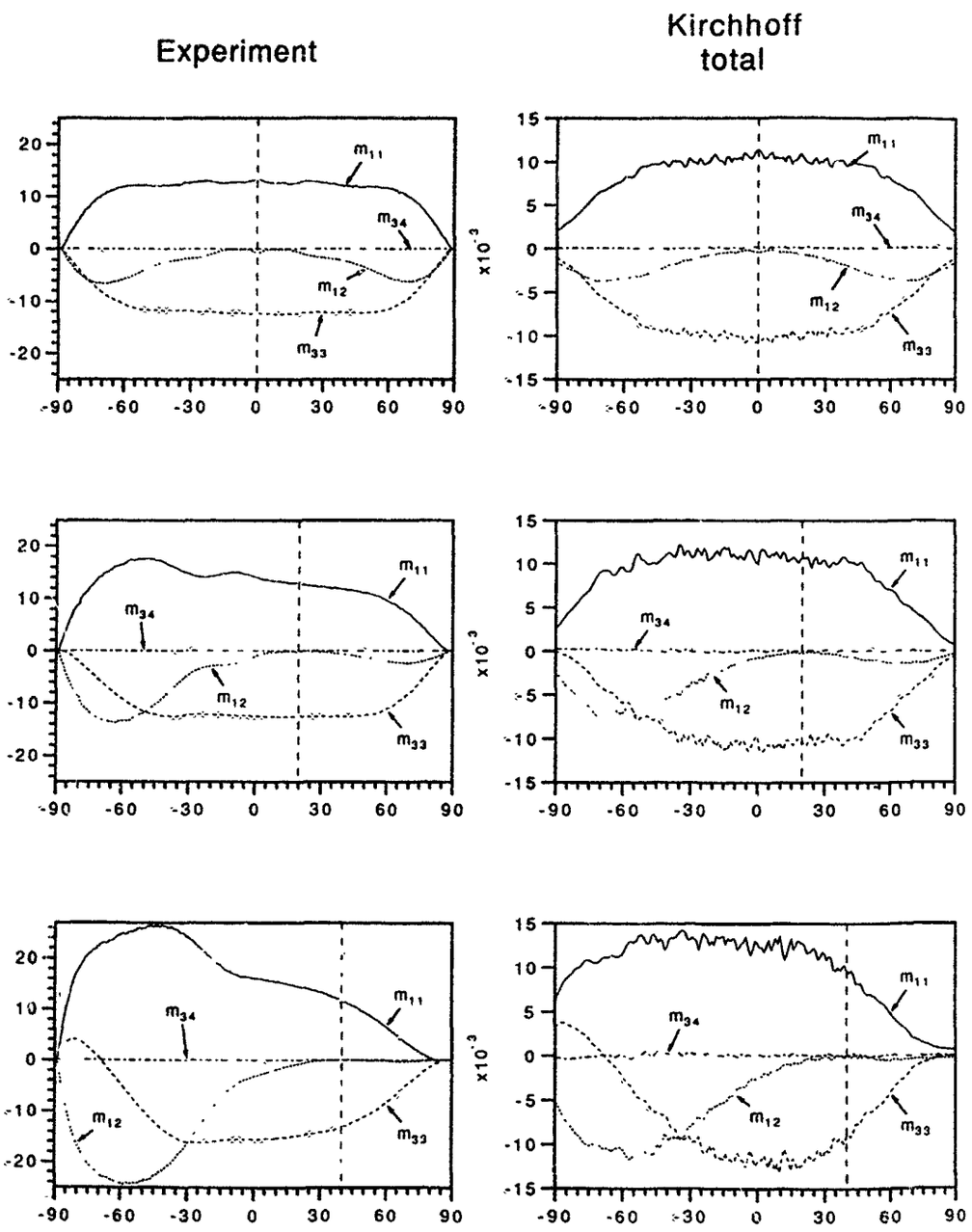

Fig. 4. As fig. 3 but for the dielectric surface #46.

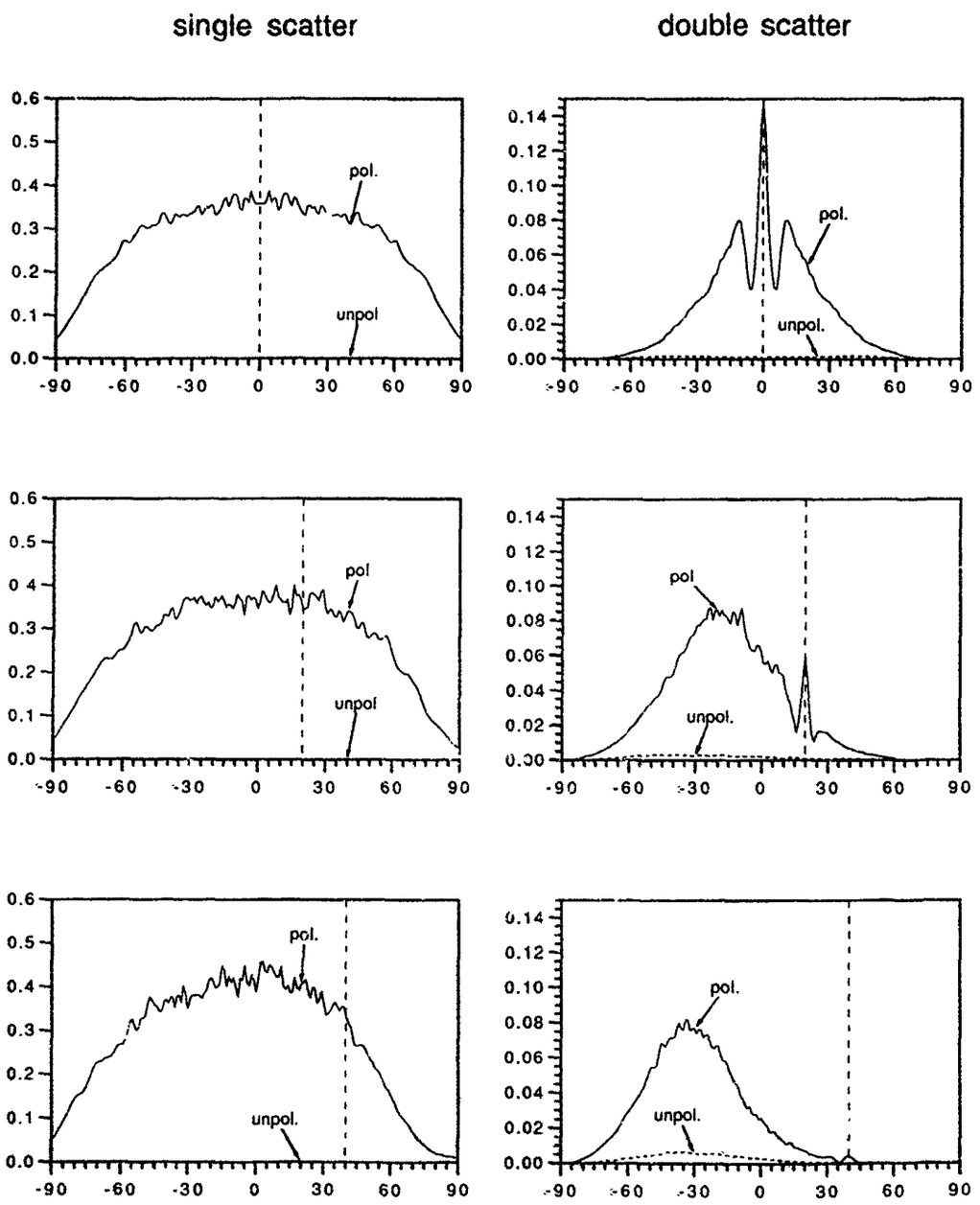

Fig. 5. Graphs of the polarised and unpolarised scatter components as a function of scatter angle for 0° incidence (top), 20° incidence (middle) and 40° incidence (bottom). Single scatter (left) and double scatter (right) for gold coated surface #46.

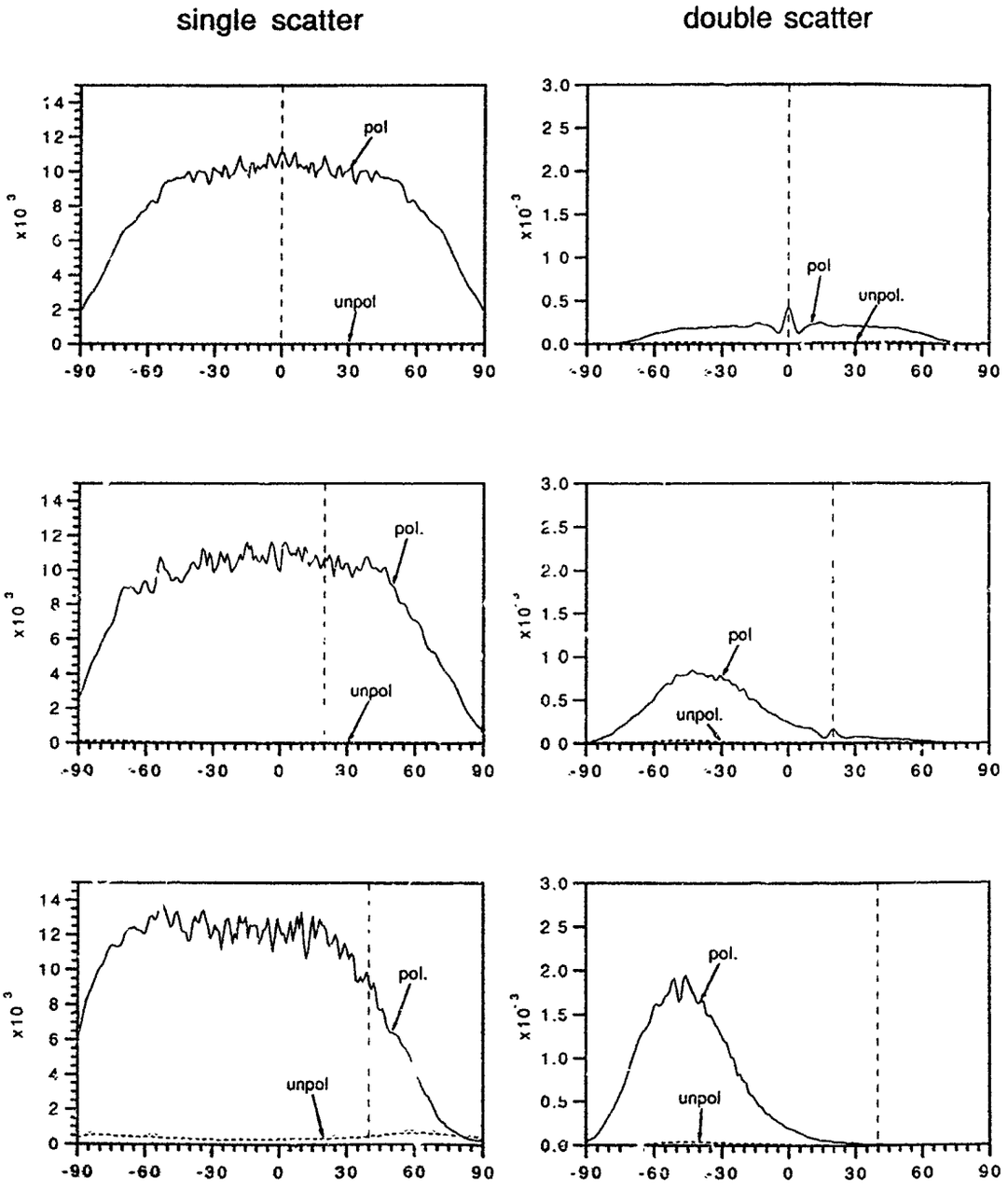

Fig. 6 As fig. 5 but for the dielectric surface #46.

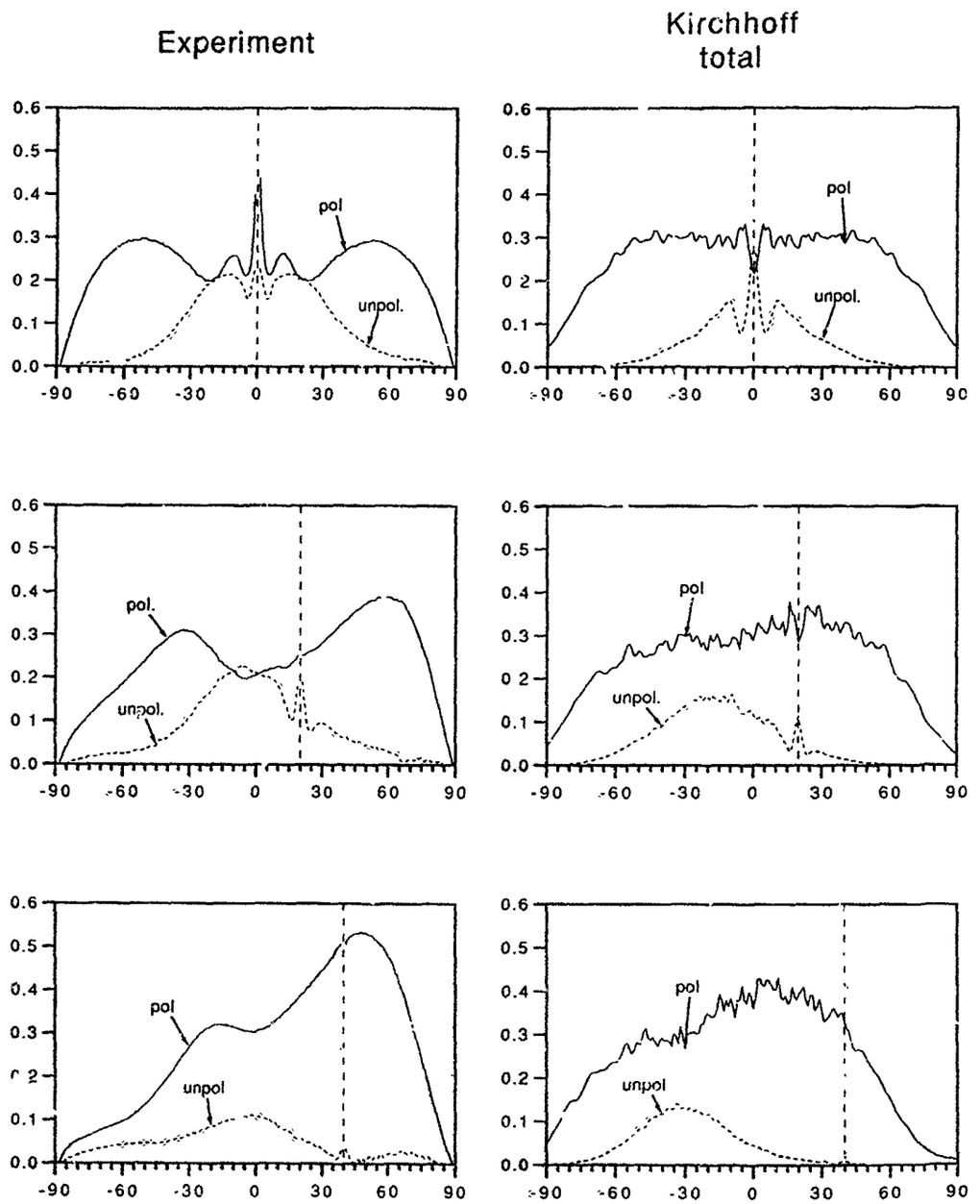

Fig. 7. Graphs of the polarised and unpolarised scatter components as a function of scatter angle for 0° incidence (top), 20° incidence (middle) and 40° incidence (bottom). Experimental results (left) and Kirchhoff total (single+double) (right) for gold coated surface #46.

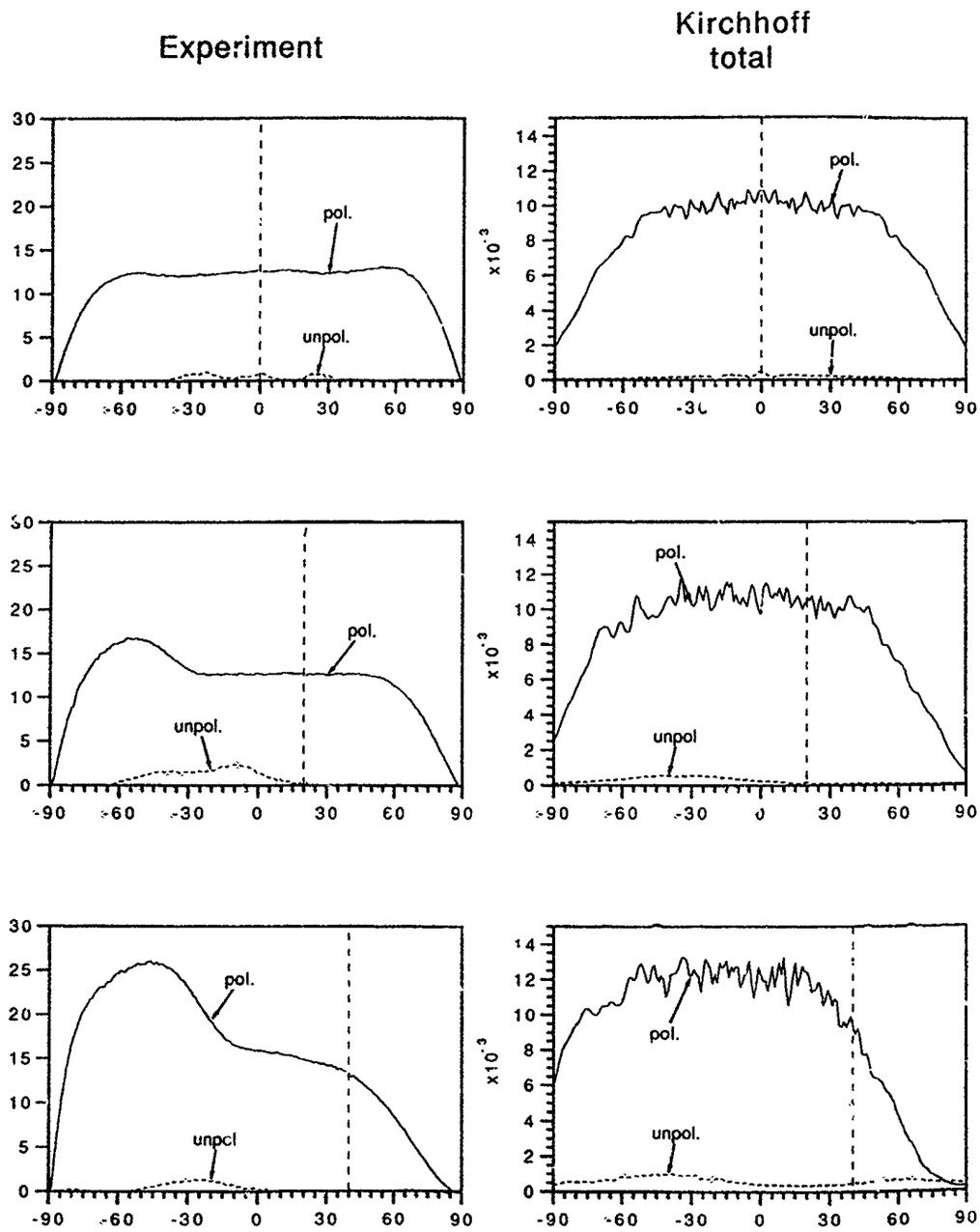

Fig. 8. As fig. 7 but for the dielectric surface #46.

the total and experimental curves. In both the gold and dielectric cases the single and double scattered intensities (figs. 5 and 6) are fully polarised whereas in the total and experimental curves (figs. 7 and 8) the gold shows a large unpolarised component and the dielectric case is again almost fully polarised. It is believed that this is caused by the partial coherence of the single and double scattered fields. Figs. 1 and 2 show that m_{33} is negative for single scatter and positive for double scatter for both materials. The experimental interpretation of m_{33} is that it represents the difference in the intensity polarised at $+45°$ and the intensity at $-45°$ for incident polarisation at $+45°$. This means that the single and double scattered fields have linearly polarised components at right angles to one another. For scattering from a perfect conductor the singly scattered field is the same polarisation as the incident field but the doubly scattered is orthogonally polarised to the incident (fig. 9). Also note that the total curves can be obtained simply by summing the single and double curves i.e. the single and double terms are largely incoherent [12–16]. Two incoherent components at right angles give a resultant field which has a varying polarisation (the phase between the two components is not fixed) [18] and so an unpolarised component results. It is important to note that the single and double scattered intensities are fully polarised but because they have components polarised in different directions and are incoherent they produce unpolarised light when combined. In the calculations the unpolarised component contains the backscatter peak since the enhancement is contained in the double scattered component and so gives an unpolarised result when combined with the single scatter term. The same effect will occur in scattering from two-dimensional surfaces for scattering in the plane of incidence although a simple geometrical effect could account for the unpolarised component out of this plane. This effect is not seen in the dielectric curves simply because the double scatter is a much smaller effect for this case. In table 1 the double scatter energy is always one or two orders of magnitude down on the single scatter for the dielectric surface so this polarisation effect will not be visible.

In fig. 7 the experimental curve shows a peak in the polarised component which is not in the calculated values. This may be due to the effect of triple scatter which gives a term polarised in the same direction as the single scatter. Even if these terms are incoherent the plane of polarisation will not vary. Therefore, since the triple scatter is expected to show an enhanced backscatter peak, a peak in the polarised component will result. The triple scatter can be expected to decrease as the angle of incidence is increased (cf. the double scatter term in refs. [12] and [13]) so that the experiment and theory become more comparable for higher angles of incidence.

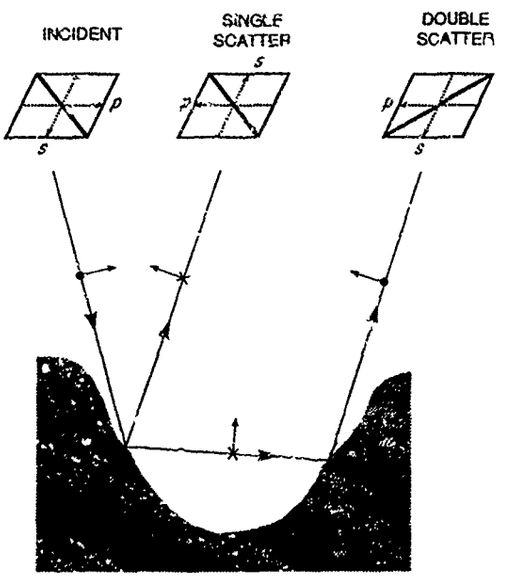

Fig. 9. Figure showing $+45°$ incident polarisation and resultant single and double scatter polarisations for a perfect conductor. The dots represent an electric field out of the plane of the diagram, the crosses an electric field into the plane. In the boxes at the top of the diagram an arrow downwards represents an s field out of the plane. Note the single scatter is co-polarised with the incident and the double scatter is cross-polarised.

4. Conclusions

The Mueller matrix for a particular surface has been calculated using the Kirchhoff method which separates the single and double scatter contributions. The advantage of using this method is seen when the difference between the polarised and unpolarised

components are calculated. The single and double scatter terms are fully polarised but the sum of the two is partially polarised for a gold coated surface since it is made up of the addition of two partially coherent components at right angles. This effect is not seen in a dielectric surface because the double scatter is too weak.

Acknowledgements

This work was supported by the Royal Signals and Radar Establishment (Malvern), the U.K. Science and Engineering Research Council (GR/F 81651) and the U.S. Army (DAJA45-90-0026).

References

[1] E.R. Mendez and K.A. O'Donnell, Optics Comm. 61 (1987) 91.
[2] K.A. O'Donnell and E.R. Mendez, J. Opt. Soc. Am. A 4 (1987) 1194.
[3] A.J. Sant, M.-J. Kim and J C. Dainty, Optics Lett. 14 (1989) 1183.
[4] M.J. Kim, J.C. Dainty, A.T. Friberg and A.J. Sant, J. Opt. Soc. Am. A 7 (1990) 569.
[5] K.A. O'Donnell and M.E. Knotts, J. Opt. Soc. Am. A 8 (1991) 1126.
[6] A.A. Maradudin, E.R. Mendez and T. Michel, Optics Lett. 14 (1989) 151.
[7] A.A. Maradudin, T. Michel, A.R. McGurn and E.R. Mendez, Ann. Phys. 203 (1990) 255.
[8] M. Nieto-Vesperinas and J.M. Soto-Crespo, Optics Lett. 12 (1987) 979.
[9] J.M. Soto-Crespo and M. Nieto-Vesperinas, J. Opt. Soc. Am. A 6 (1989) 367.
[10] M. Saillard and D. Maystre, J. Opt Soc. Am. A 7 (1990) 982.
[11] W.S. Bickel and W.M. Bailey, Am J Phys 53 (1985) 468
[12] N.C. Bruce and J.C. Dainty, J. Mod. Optics 38 (1991) 579.
[13] N.C. Bruce and J.C. Dainty, J. Mod. Optics 38 (1991) 1471.
[14] J.S. Chen and A. Ishimaru, J. Acoust. Soc Am. 88 (1990) 1846.
[15] A. Ishimaru and J.S. Chen, J. Acoust. Soc. Am. 88 (1990) 1877.
[16] A. Ishimaru and J.S. Chen, Waves in Random Media 1 (1991) 21.
[17] A.J. Sant, Enhanced backscattering of light from randomly rough diffusers, Ph. D. thesis (Univ of London, 1991).
[18] W.A. Shurcliff, Polarized light (Oxford University Press, Oxford, 1962).
[19] M. Born and E. Wolf, Principles of optics (Pergammon Press, Oxford, 1987)

OP5.3

THEORY AND MEASUREMENTS OF THE ANGULAR CORRELATION OF SPECKLE PATTERNS

R W Syratt, J C Dainty
Imperial College, London

In this work, we illuminate a randomly rough surface at one angle, θ_1, record the intensity around a small range of angles centered on another angle θ'_1 and repeat this process for another angle of illumination and viewing, θ and θ'. The two recorded speckle patterns are then cross-correlated to obtain the correlation coefficient between them.

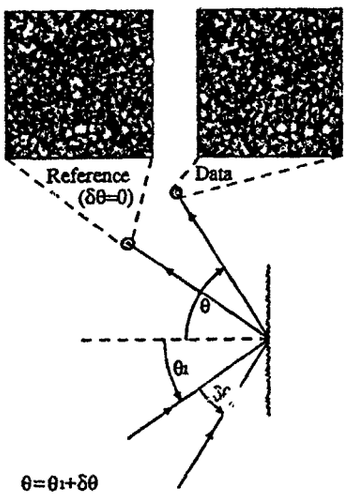

Figure 1

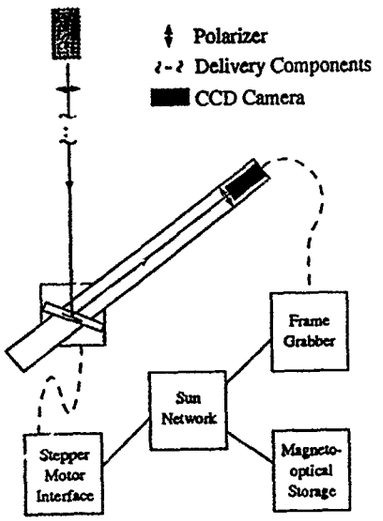

Figure 2

The work conducted so far is limited to observation in the specular direction ($\theta'_1 = \theta_1$, $\theta' = \theta$) this ensures a large correlation range, but limits the technique to examination of surfaces which do not reflect a large specular component. The geometry can be seen in Figure 1. A range of speckle patterns (changing $\delta\theta$) is correlated with a fixed reference pattern (θ_1).

Figure 2 schematically shows the experimental equipment; typically twenty-five speckle images are taken from the charge-coupled-device (CCD) camera and averaged to reduce measurement noise. The optical disk is necessary to store the vast amounts of data gathered.

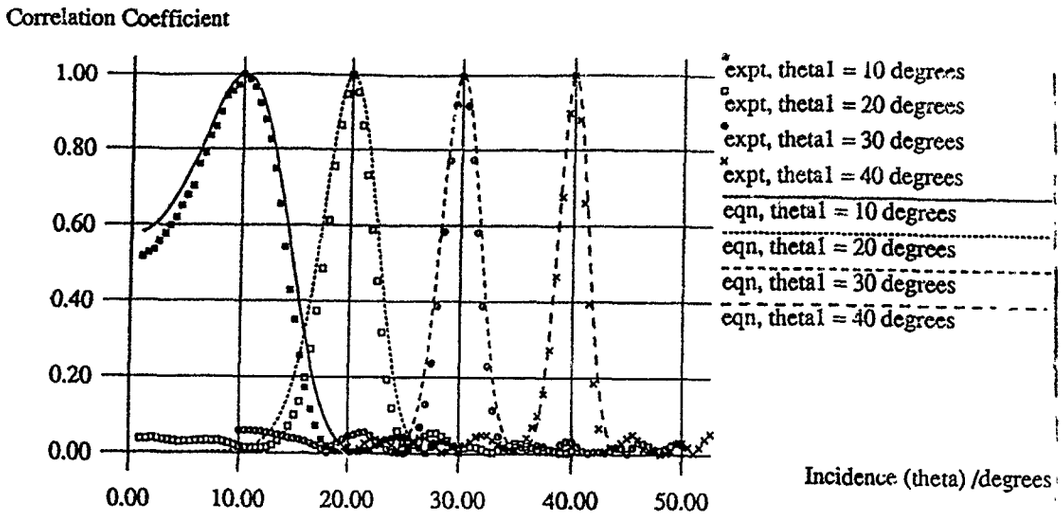

Figure 3

Graphs of experimental angular correlation curves at different references angles, for a Gaussian random rough surface — with an rms height (σ) of $2.27 \pm 0.2\mu m$ and correlation length of $20.7 \pm 0.2\mu m$ — illuminated by a HeNe laser of wavelength (λ) $0.633\,\mu m$ are given in Figure 3; these are computationally calculated from the speckle images. Overlaying them are the curves from an equation derived from the single scatter Kirchoff approximation, a form of which is given by equation 1. In practice a more general two dimensional equation is used and averaged over the field view of the CCD camera.

$$C(\theta_1, \delta\theta) = \frac{\cos^2\theta_1}{\cos^2(\theta_1 + \delta\theta)} \exp\left[-\left(\frac{4\pi\sigma}{\lambda}\right)^2 \left(\cos\theta_1 - \cos^2(\theta_1 + \delta\theta)\right)^2 \right] \qquad (1)$$

References

[1] D Leger, E Mathieu, J C Perin, "Optical Surface Roughness Determination Using Speckle Correlation Technique", Applied Optics, 14 872-877 (1975)

[2] D Leger, J C Perrin, "Real Time measurement of surface roughness by correlation of speckle patterns", J.opt.Soc.Am.,66,1210-1217 (1976)

OP1.5

SCATTERING FROM DENSE VOLUMES

N C Bruce
Imperial College, London

Introduction

There has recently been a great deal of interest in the use of light for non-invasive testing in medicine. Possible applications include mammography, investigation of skin cancers and detection of cancerous tissue during surgery. The use of optics in a clinical environment requires compact, robust devices which are possible by using fibre optics. An experimental model of such a, device has been built and its response for different experimental conditions studied.

Experiment

The experimental arrangement is shown schematically below.

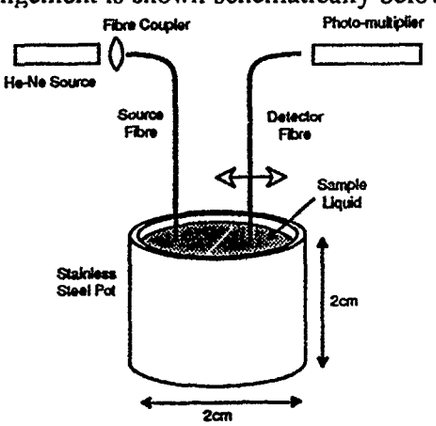

Light from a He-Ne laser is delivered to the sample via a mono-mode fibre to give a clean illumination spot in the sample. A multi-mode fibre is used to collect the scattered light and deliver it to a photon counting photo-multiplier connected to a computer. The detection fibre is scanned away from the source fibre, always in the same plane. The sample holder was a stainless steel pot of $2cm$ diameter. This pot was large enough so that the effect of reflections from the edge was negligible. The samples used were collections of polystyrene spheres in water obtained from Sigma Chemical Company. The samples were 10% by volume concentration of particles of diameters $0.091\mu m$, $0.296\mu m$, $0.46\mu m$,, $0.605\mu m$ and $0.778\mu m$. Water was added to some of these samples to give 1% volume density liquids. Since these samples are so well characterised it will be possible to compare the experimental results with theoretical values.

Results

The figures below show the number of counts per second versus separation of the two fibres for the 10% and 1% volume density samples for the 0.091 μm,

0.46μm, and the 0.778μm particles.

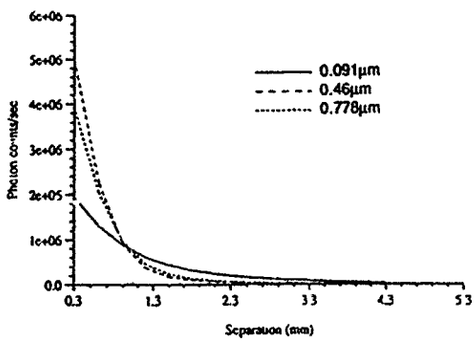

10% volume density

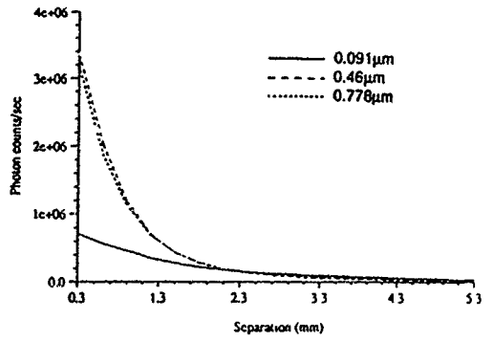

1% volume density

From these curves it can be seen that there is no linear relationship between the width or the maximum value of the scatter pattern and the size of the particle. Indeed from the diffusion theory [1] the figure that describes the scattering is the product of the number of particles per unit volume, the scattering cross section per particle and 1 minus the average of the cosine of the scattering angle. For the particles of interest here Mie theory gives values for this product of 7.43mm^{-1}, 38.42mm^{-1}, 42.81mm^{-1}, 38.50mm^{-1} and 33.90mm^{-1} for increasing particle size and the 10% case. The 1% values are simply a 10th of these. From the figures scatter patterns follow the general behaviour of this parameter, the smallest particle giving the smallest signal and the middle sized the largest.

Work is progressing to perform the experiments for a wavelength of 830nm (which is more suitable for medical applications) and to obtain calculations of the expected scatter pattern using the diffusion approximation.

Reference

[1] R A J Groenhuis, H A Ferwerda, J J Ten Bosch Scattering and absorption of turbid materials determined from reflection measurements App.Opt.,22,(1983),2456.

Presented at "ICO-16", Budapest, 9-13 August '93

Measurements of angular scattering by rough surfaces at grazing incidence

V. Ruiz Cortés and J.C. Dainty

Applied Optics Section. Blackett Laboratory.
Imperial College of Science, Technology and Medicine
Prince Consort Road, London SW7 2BZ, U.K.

ABSTRACT

An experimental study of light scattering at grazing incidence from random rough surfaces is presented. The surfaces are fabricated in photoresist and gold-coated.

2. INTRODUCTION

The interaction between light and matter has been studied for several years. The reflection and refraction of light in a plane surface of any material are well known phenomena and it is possible to obtain information about material properties by analysing the reflected and refracted light. However, the interaction of light with rough surface is, in general, a non-resolved problem. In the last few years significant advances have been made in the study of light scattered from rough surfaces. Of special interest has been multiple scattering effects [1] at normal and small angles of incidence (up to approx. 50° from the normal). Little work has been done at grazing incidence where the current theories are no longer valid. Furthermore, the available data at such angles of incidence does not include accurate information about the surface structure. The study of rough surface scattering at grazing incidence has many potential applications, such as radar.

3. LIGHT SCATTERING

For scalar wave fields at arbitrary angles of incidence the scattered field is described by the Helmholtz integral formula [2]

$$\Psi_s(\vec{r}_o) = \frac{1}{4\pi}\int_s\int\left\{G(\vec{r}_o,\vec{r}')\frac{\partial\Psi(\vec{r}')}{\partial n} - \Psi(\vec{r}')\frac{\partial G(\vec{r}_o,\vec{r}')}{\partial n}\right\}ds'$$

where $\Psi_s(\vec{r}_o)$ is the scattered field at any arbitrary point $\vec{r}_o$ in the medium, $\Psi(\vec{r}')$ is the incident field on the surface, $\partial/\partial n$ is the derivative along the normal component and $G(\vec{r}_o,\vec{r}')$ is the free space Green's function.

Different approximation methods have been used to solve this integral equation such as Perturbation Theory [3] for small surface heights and the Kirchhoff Approximation [2] for small slopes, each of these methods have a range of validity depending on the parameters of the rough surface. However some methods fail at large angles of incidence (greater than 50°) or others, due to computer implementation, are excessive time-consuming programs. To avoid these problems for grazing incidence it is possible to apply the Parabolic Approximation Method [4].

At grazing incidence the scattered field propagates predominantly in one direction (fig 1), it has a slow varying component in the z-axis and this fact is used for the parabolic approximation to redefine the Green's function by a direct approximation of the free space function which for a 2-D geometry is given by[4]:

$$G(x,z;x'z') = \frac{1}{2}\sqrt{\frac{i}{2\pi k(x-x')}}\exp\left[\frac{ik(z-z')^2}{2(x-x')}\right]$$

With this approximation we solve the Helmholtz integral equation and we obtain an expression for the scattered field, of course this method is inapplicable to situations in which backscattering is significant.

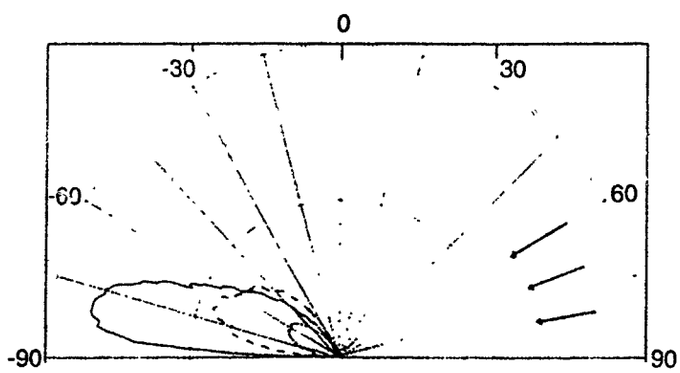

Figure 1.- Measured diffuse scattering at different angles of incidence (60°, 70° and 80°) from a rough surface with standard deviation $\sigma_h = 2.27\mu m$ and correlation length $a = 20.9\mu m$.

4. ACKNOWLEDGMENTS

One of us (V. Ruiz Cortés) was supported by a CONACYT and CICESE scholarship.

5. REFERENCES

1.-K.A. O'Donnell and E.R. Méndez, "Experimental study of scattering from characterized random surfaces", J. Opt. Soc. Am. Vol A4, pp. 1194-1196, 1987.

2.-P. Beckmann and A. Spizzichino, "The Scattering of Electromagnetic Waves from Rough Surfaces", Pergamon Oxford.

3.-A.R. McGurn, et al., "Localization effects in the scattering of light from randomly rough grating", Phys. Rev. Vol. B31, pp. 4866-4871, 1985.

4.-M. Spivack, "A numerical approach to rough-surface scattering by the parabolic equation method", J. Acoust. Soc. Am. Vol 87, pp 1999-2004, 1990.

Optics Communications 106 (1994) 123–126
North-Holland

OPTICS
COMMUNICATIONS

Calculations of grazing incidence scattering from random rough surfaces using the Kirchhoff approximation

N.C. Bruce, V. Ruiz-Cortés and J.C. Dainty

Blackett Laboratory, Imperial College, London SW7 2BZ, UK

Received 11 October 1993

A simple numerical method based on the Kirchhoff approximation with shadowing is presented for the calculation of the scattered intensity distribution for rough surfaces illuminated at angles up to ≈ 85° incidence. It may be possible to go to higher angles but many more discretisation points are required on the surface. The method is valid for a wide range of roughness values which is an advantage over other methods.

1. Introduction

Scattering of electromagnetic waves from rough surfaces for high angles of incidence has proved to be a difficult problem to calculate. The situation is of interest particularly for scattering of radar from the sea surface where the incidence angle is within a few degrees of grazing [1]. Calculations for this situation have proved very difficult although some have been done. The parabolic equation method [2–4] has been used to calculate from very near grazing incidence but it is limited to surfaces with height variations less than approximately one-fifth of a wavelength of the illuminating radiation. The small perturbation method [5] has also been used but it is limited to even smaller variations of the surface heights.

In this communication the single scatter Kirchhoff approximation with shadowing [6–11] is used to calculate the scattered intensity patterns for high angles of incidence. The physical justification for using this approach is that at high incidence most of the surface will be in shadow and only the high parts of the surface will be scattering. Since these will tend to be flat (as they will be maxima of the surface) the light will tend to be scattered away from the surface. Hence only the single scatter term is required. The results are compared to experimental results and the variation of the scattered intensity with changing roughness is presented to show that the method is valid for rougher surfaces.

2. Theory

The required results are derived from the two-dimensional Helmholtz integral equation for the scattered field (the surface profile is constant along the y-direction)

$$E_s(x,z) = \frac{1}{4\mathrm{i}} \int_r \left(E_t(x',z') \frac{\partial H_0^{(1)}(kr)}{\partial n} - H_0^{(1)}(kr) \frac{\partial E_t(x',z')}{\partial n} \right) \mathrm{d}s', \tag{1}$$

where $E_t(x',z')$ is the total field at the point (x',z'), $r = [(x-x')^2 + (z-z')^2]^{1/2}$, $H_0^{(1)}(kr)$ is the zeroth order Hankel function of the first kind and $\mathrm{d}s'$ is an element of the surface.

The Kirchhoff Approximation approximates the total field on the surface as the sum of the incident field plus the reflected field at that point

$$E_t(x,z) = (1+R)\,E_i(x,z), \tag{2}$$

$$\frac{\partial E_t(x,z)}{\partial n} = \mathrm{i}(1-R)\,\boldsymbol{k}_i \cdot \boldsymbol{n}\, E_i(x,z), \tag{3}$$

where R is the planar reflection coefficient, at the point (x,z), which depends on the local incidence angle, $E_i(x,z)$ is the field incident at that point, $\boldsymbol{k}_i$ is the incident wave-vector and $\boldsymbol{n}$ is the outward normal to the surface at that point. The condition for validity of the approximation is immediately obvious from

SSDI 0030-4018(94)00054-X

above since R is the *planar* reflection coefficient. The surface must be locally flat or, as is usually written, the radius of curvature of the surface must be large compared to the wavelength.

Substituting (2) and (3) into (1) and proceeding as in Beckmann [12] the standard single scatter solution can be written as

$$\varphi_{sc}^{\infty}(\theta_i,\theta) = \frac{1}{4}\sqrt{\frac{2}{\pi k_0 r}}\exp[i(k_0 r - \pi/4)] \times \int_{\Gamma} \exp\{i[\{k_0(\sin\theta_i - \sin\theta)\,x - k_0(\cos\theta_i + \cos\theta)\,h(x)\}\} \times [-k_0(\sin\theta + \sin\theta_i)\,h'(x) + k_0(\cos\theta - \cos\theta_i) - R(x,z)\,k_0(\sin\theta - \sin\theta_i)\,h'(x) + R(x,z)\,k_0(\cos\theta + \cos\theta_i)]\,dx, \quad (4)$$

where the reflectivity $R(x', z')$ is a function of x since the local angle of incidence varies along the surface. In eq. (4), Γ represents the surface profile, θ_i is the incidence angle, θ is the angle of scatter (measured positive in the opposite sense to the incident angle). $R(x, z)$ is, in the general case given by the Fresnel reflection coefficients. To obtain this expression we have assumed an incident plane wave of unit amplitude. When the Kirchhoff method is used this expression is usually simplified by integration by parts [6–9]. However this process leads to two terms, one of which is an edge effect term which is neglected [6–9]. In the situations of very nearly grazing incidence this edge term is not negligible, so the calculation proceeds from a discretisation of the above equation. This involves splitting the integral into a summation of values which are constant over a small region of the variable x. This equation is the first term in the iterative solution method [13]; however, to obtain a physically realistic result the effects of shadowing must be included. This is particularly true for the case of grazing incidence when a large fraction of the surface is not illuminated because the incident light is blocked by other parts of the surface. These effects are included by multiplying the integrand in (4) by incidence and scatter shadow functions

$S(x', z') = 1$, if (x', z') is illuminated,

$= 0$, if (x', z') is not illuminated,

$S'(x', z') = 1$, if (x', z') is visible,

$= 0$, if (x', z') is not visible.

These represent geometrical or straight line shadow functions and so are an approximation to the true effect of shadowing. Equation (4) was discretised by assuming that the integrand is constant over a suitably small range of the surface profile. Then the integral can be replaced by a summation and the system can be programmed into a computer. To remove speckle noise the calculations are performed for many surfaces of the same statistics and the resulting intensity patterns averaged.

It should be pointed out that the inclusion of the shadowing explicitly is essential for the method to work for grazing incidence. It was found that for grazing incidence many more points were required in the discretisation of the surface profile to follow the phase variations of the incident field on the surface. This means that the second (and higher) order terms in the iterative series solution (i.e. without the inclusion of the shadowing explicitly) would take too long to compute on even the fastest computers. This is important since it was shown [13] that, for the iterative solution, if an incident ray is blocked by n other points before it can reach a particular point on the surface the n'th iteration is required to account for the shadowing. For example in fig. 1 the ray shown is blocked by points A, B, C and D before reaching point E. Hence the fourth order iteration would be required to give the correct scattered field from point E. For grazing incidence light will tend to be blocked by many points and so very high orders in the iterative series would have to be computed to give an accurate

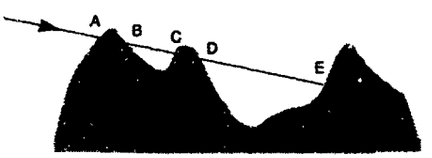

Fig. 1. Shadowing at large angles of incidence. The incident ray that is in the direction of point E is blocked by the four points A, B, C and D.

result. Therefore, although the method presented here is an approximation to the iterative solution, it is a practical solution whereas computer time limitations are prohibitive for the iterative method.

3. Results

In this section results are presented and compared with experimental data. The calculations were performed for a one-dimensional perfectly conducting surface and for a metal surface but only the perfectly conducting surface results are presented. For the metal case there was no difference in the normalised curves for the two polarisations although the absolute value of the scattered energy was higher for the s polarised case (electric vector perpendicular to the scattering plane) than the p polarised case. This is due simply to the fact that the Fresnel reflection coefficients are larger for s. The normalised curves were very similar to the perfect conductor case. For a perfect conductor the scattered intensity is the same for the two fundamental polarisations, s and p, and the modulus of the reflection coefficient is 1.

The surface used here is approximately described by a gaussian correlation function with a 1/e distance $\tau = 12.0$ μm and a gaussian distribution of heights with a standard deviation of $\sigma = 0.40$ μm. The experiments were conducted with a helium-neon laser ($\lambda = 0.633$ μm). The calculations were performed on a 400λ length of surface discretised into 1000 points. On a Sun Sparc station the calculations took 40 minutes per frame. As a check on the validity of the calculation the ratio of the scattered energy and the incident energy was found. This is termed the unitarity as it should have the value 1 for a perfect calculation (as all the energy is reflected from a perfectly conducting surface). The unitarities were: for 60° incidence = 1.0089; for 70° = 0.9978 and for 80° = 1.0436. These numbers compare well with results for other situations [6–8] and give confidence in the shape of the resulting curves.

Figure 2 shows the comparison between calculations and experimental results for the normalised intensity (the graphs are normalized to have unit area under the curve). Note that the experimental results are for a surface rough in both the x and y directions whereas the calculation is for a surface rough in the x direction and constant in the y direction. This means that the quantitative comparison of the results may not be valid. However, the qualitative comparison can be useful. As can be seen from the figure these curves for the scattered light distributions as functions of angle agree well with the experimental data. In particular the presence of the large specular peak at 80° incidence is predicted in the calculations.

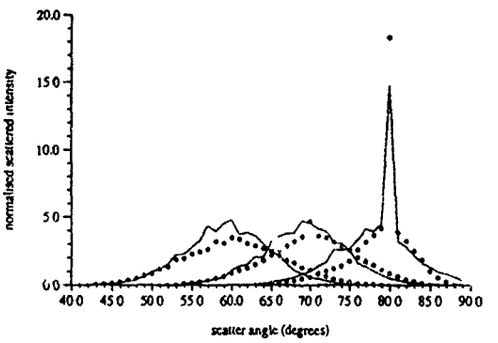

Fig. 2. Comparison of experiments and calculations for 60°, 70° and 80° incidence on a surface with $\sigma = 0.4$ μm and $\tau = 12.0$ μm. Solid lines are the calculation and circles are the experimentally measured values for p polarisation incident and detected. All curves are normalised to unit area.

For higher angles of incidence the calculations the method starts to break down. The values for the unitarity are 1.02 for 85° incidence, 1.06 for 86°, 1.20 for 87° and 2.51 for 89°. Therefore for the values of the surface parameters used the method described here may be used for incidence angles of up to approximately 86°. It may be that very many extra points are required for the large angles of incidence to follow the phase of the incident wave on the surface.

In the computer it is possible to increase the roughness of the surface by increasing the value of σ. Figure 3 shows the normalised scattered intensity patterns for four surfaces all with the same value of $\tau = 12.0$ μm as for the surface above and values of the roughness of (a) $\sigma = 0.40$ μm, (b) $\sigma = 0.8$ μm, (c) $\sigma = 1.2$ μm and (d) $\sigma = 1.6$ μm. The incidence angle is 80° for the curves shown. The unitarities for the calculations were (a) 1.0436, (b) 0.96, (c) 0.998 and (d) 1.02. All of these numbers are reasonable and show that the calculation is less sensitive to the roughness than it is to the angle of incidence when the incidence angle is high. This is true since most of the surface is shadowed

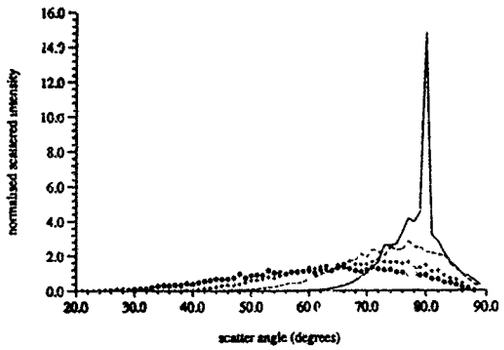

Fig. 3. Calculated variation of scattering for increasing roughness. The angle of incidence is 80°. The solid line is for $\sigma = 0.4$ μm, the dashed line for $\sigma = 0.8$ μm, the crosses for $\sigma = 1.2$ μm and the circles for $\sigma = 1.6$ μm, all for $\tau = 12.0$ μm.

at these high angles of incidence and only the topmost parts of the surface contribute to the scattered field. These parts will be reasonably flat for a wide range of roughness values so that the method should be valid for many values of σ. An interesting point to note from from these curves is that as the roughness is increased the maximum in the scattered intensity distribution moves to lower angles. This arises because the parts of the surface which are illuminated are either horizontal or sloped slightly towards the illuminating direction (as slopes in the opposite direction will be shadowed). Therefore as the roughness is increased the slopes of these parts of the surface will become steeper and, according to a simple geometrical picture, more light will be directed towards smaller scatter angles.

4. Conclusions

A numerical method has been presented to calculate the scattered intensity distribution for grazing incidence scattering from rough surfaces. The method is valid for incidence angles up to $\approx 85°$ and for surfaces whose rms roughness is up to a few wavelengths and can be used to calculate the scattered intensity for any material of rough surface. The method has the virtue of simplicity and seems to agree with experimental data.

Acknowledgements

This work was supported by grants from the U.K. Science and Engineering Research Council (GR/F81651) and the U.S. Army Research Office (DAJA45-90-C-0026). VRC thanks CONACYT and CICESE in México for financial support.

References

[1] H.F. Helmken, I.E.E Proceedings 137 (1990) 113.
[2] M. Spivak, J. Acoust. Soc. Am. 87 (1990) 1099.
[3] M. Spivak, J. Opt. Soc. Am. A 9 (1992) 1252.
[4] M. Spivak, J. Phys. A: Math. Gen. 25 (1992) 3295.
[5] J.M. Soto-Crespo, M. Nieto-Vesperinas and A.T. Friberg, J. Opt. Soc. Am. A 7 (1990) 1185.
[6] N.C. Bruce and J.C. Dainty, J. Mod. Optics 38 (1991) 579.
[7] N.C. Bruce and J.C. Dainty, J. Mod. Optics 38 (1991) 1471.
[8] N.C. Bruce, A.J. Sant and J.C. Dainty, Optics Comm. 88 (1992) 471.
[9] J.S. Chen and A. Ishimaru, J. Acoust. Soc. Am. 88 (1990) 1846.
[10] A. Ishimaru and J.S. Chen, J. Acoust. Soc. Am. 88 (1990) 1877.
[11] A. Ishimaru and J.S. Chen, Waves in Random Media 1 (1991) 21.
[12] P. Beckmann and A. Spizzichino, The scattering of electro-magnetic waves from rough surfaces (Pergamon, New York, 1963).
[13] E. Liszka and J. McCoy, J. Acoust. Soc. Am. 71 (1982) 1093.